Fluids and Barriers of the CNS

RESEARCH

Open Access

BBB proteomic analysis reveals that complex febrile seizures in infancy enhance susceptibility to epilepsy in adulthood through dysregulation of ECM-receptor interaction signaling pathway

Qian Wang[1,2], Liangyu Pan[1,2], Siruan Chen[1,2], Yuyu Zhang[1,2], Guangyuan Liu[1,2], Yiying Wu[1,2], Xia Qin[1,2], Panpan Zhang[1,2], Wei Zhang[1,2,3*], Jianghua Zhang[1,2*] and Dezhi Kong[1,2,3*]

Abstract

Background Complex febrile seizures (CFS) have been associated with an increased risk of epilepsy in adulthood. However, the specific link between blood-brain barrier (BBB) and the predisposition to epilepsy in adults who experienced CFS during infancy remains unclear. The objective of this study was to investigate the alteration of BBB in adult mice who had experienced CFS during infancy, and to explore the mechanisms of increased susceptibility to epilepsy after CFS.

Methods The CFS pup model was induced using hot air, and the seizure susceptibility was examined using low-dose pentylenetetrazole (PTZ) after 8 W. The brain microvessels representing BBB function were isolated and their protein expression changes were analyzed using data-independent acquisition (DIA) proteomic techniques. Subsequently, the bioinformatic analyses were performed using ClusterProfiler, STRING, Gene Set Enrichment Analysis (GSEA), etc. The enriched pathways, changes in the expression of BBB-related proteins, and alterations in metabolites including certain neurotransmitters were subsequently validated by Western Blotting, quantitative real-time polymerase chain reaction (qRT-PCR), and mass spectrometric imaging (MSI). In addition, we selected the MMP inhibitor Incyclinide to verify that dysregulation of the ECM-receptor interaction signaling pathway increases epilepsy susceptibility in adult mice.

Results Mice that experienced CFS in infancy show increased susceptibility to epilepsy in adulthood, and BBB proteomic profile was significantly altered in the CFS mice. The network analysis suggests that dysregulation of

*Correspondence:
Wei Zhang
weizhang@hebmu.edu.cn
Jianghua Zhang
zhangjianghua@hebmu.edu.cn
Dezhi Kong
kongdezhi@hebmu.edu.cn

Full list of author information is available at the end of the article

the extracellular matrix (ECM)-receptor interaction pathway is a key mechanism. Moreover, MSI analysis uncovered notable changes in differential metabolites, including amino acids and nucleotide-derived neurotransmitters associated with the function of BBB maintaining neuronal homeostasis. Subsequent validation experiments showed that dysregulation of the ECM-receptor interaction signaling pathway exacerbated epilepsy susceptibility in adult mice.

Conclusion Our research represents the pioneering demonstration of the modified BBB proteomics associated with epilepsy susceptibility in adult mice previously exposed to CFS in infancy. Notably, the increased susceptibility is attributed to the dysregulation of the ECM-receptor interaction pathway. These findings may help to elucidate the role of BBB alterations in the progression of epilepsy susceptibility, and provide new orientations for subsequent prevention and treatment of epilepsy.

Keywords Complex febrile seizures, Susceptibility to epilepsy, Blood-brain barrier, Proteomic analysis, ECM-receptor interactions

Introduction

Febrile seizures (FS) are a convulsive disorder in children, characterized by an abnormal increase in neuronal excitability and typically triggered by a rapid rise in body temperature during a fever [1]. Currently, FS occur in 3–5% of the world's population of children aged 3 months to 5 years [2]. Studies have shown that complex febrile seizures (CFS) significantly increase the risk of developing epilepsy later in life, with children who experience CFS being ten times more likely to develop epilepsy compared to those who do not have FS [3]. Especially, CFS prone to develop into epilepsy thus affecting the patient's long-term quality of life [4, 5]. However, it is unclear how infantile CFS cause to adult epilepsy; therefore, exploring the mechanisms of epilepsy susceptibility after CFS is key to preventing the development of epilepsy for adults.

Shortly after neovascularization, endothelial cells of brain capillaries are connected through tight junctions (TJs) and adhesion junctions thereby forming the blood-brain barrier (BBB) [6]. BBB protects the neuronal microenvironment and regulates brain homeostasis under physiological conditions, and exerts an important influence on neuronal excitability, connected synaptic structure and function under pathological conditions [7]. Several studies have shown that cerebral capillary endothelial cells have unique biological functions that are critical for maintaining central nervous system (CNS) homeostasis [8]. This emphasizes the crucial role of cerebral capillary transport in the BBB function. Moreover, FS induce an inflammatory response in the body's immune system, prompting microglia to release cytokines that exacerbate BBB leakage and allow cytokines to enter CNS, aggravating the development of seizures [9, 10]. Several researchers have noted a correlation between pediatric seizures and alterations in the BBB. Specifically, vasogenic edema resulting from prolonged FS is a sign of BBB disruption [11]. Also, BBB dysfunction has been recognized as a risk factor in the development of epilepsy [12]. These findings suggest the potential role of altered BBB structure and function in seizures and epilepsy. Nevertheless, how specific alterations of the BBB during CFS to increase the susceptibility to epilepsy remains uncertain.

Cerebral capillaries make up only 0.1% of the total brain volume, but they play a crucial role in maintaining the BBB [13, 14]. Proteomic analysis can help uncover protein expression levels in both the normal physiology of the BBB and in pathological states. In our study, we evaluated the susceptibility to epilepsy through pentylenetetrazole (PTZ) induced seizures in adult C57BL/6 mice that had experienced CFS in infancy. For the first time, we investigated molecular mechanisms in the BBB related to epilepsy susceptibility using proteomic analysis of isolated brain capillaries. Our study may help to elucidate the role of BBB alterations in the progression of epilepsy susceptibility in adulthood, and provide new orientations for subsequent prevention and treatment of epilepsy.

Materials and methods

Animals and experimental groups

C57BL/6 mice were purchased from Beijing Spefo Biotechnology Co. Ltd. (Beijing, China). The animals were housed in a temperature-controlled room with free access to food and water during a 12-hour light-dark cycle. Animal experiments were conducted in strict accordance with the Animal Care Guidelines approved by the Institutional Animal Care and Use Committee of Hebei Medical University (Approval Number: IACUC-Hebmu-2021022, Shijiazhuang, China). All experimental procedures were meticulously designed and executed to minimize pain and the overall number of animals used, following the basic guidelines set forth by the Laboratory Animal Management Center of Hebei Medical University.

The mouse pups were randomly divided into two groups following strict experimental protocols. The birth day of C57BL/6 mice was designated as postnatal

day 0 (P0), and hot-air-induced CFS modeling was conducted on postnatal day 10–11 (P10-11) mouse pups. The remaining pups from the same litter were used as the control group.

CFS treatment and behavioral analysis

Experimental CFS models use methods adapted from previous studies [15–18]. The experiment was conducted from 10:00 am to 05:00 pm. The oven was preheated for 30 min in advance. One liter glass beaker was placed inside the oven with a moderately warm airflow over the top, located 50 cm from the bottom of the beaker. The temperature of the oven was closely monitored using a digital thermometer to ensure it did not exceed 50 °C. Once the temperature inside the beakers reached 43 ± 0.5 °C, C57BL/6 mouse pups (P10-11) were gently placed in the bottom of the beakers until a convulsive seizure was induced. Pups that did not experience a seizure within 55 min were excluded from further experiments. The times and temperature characteristics of convulsive grand mal seizures were then calculated (Table 1). Wherein, once a convulsive seizure was induced, the animal was removed from the oven to a cool surface for 2 min, and the pups were returned to the oven and the process repeated for at least 30 min. Observation was carried out for an additional 15 min, and the mouse pups were returned to their mother's living cage. The control animals ($n = 8$) were operated as described above, except that they were not exposed to high-temperature conditions. The severity of convulsive seizures was categorized according to the Racine grading scale: Grade I facial clonus, including blinking, whisker movement, and rhythmic chewing; Grade II: Grade I plus rhythmic head nodding; Grade III: Grade II plus myoclonus of the forelimbs, but no hind limb upright position; Grade IV: Grade III plus hind limb upright position; Grade V full-blown tonic-clonic seizure with loss of postural control. Mice with two seizures of grade V and above were defined as successful CFS modeling ($n = 12$). The two pups had only one V-shaped episode in 55 min, which was removed.

Table 1 Hyperthermia and seizure characteristics in C57BL/6J mice

	HT ($n = 12$)	CON ($n = 8$)
Days	10–11	10–11
Weight at P10-11 (g)	4.77 ± 0.54	4.69 ± 0.67
Threshold temperature(°C)	43 ± 1.5	RT
Animals with seizures (%)	100	NA
Tonic-clonic seizure latency (min)	12 ± 3	NA
The number of tonic-clonic seizures	3 ± 1	NA
Number of deaths	2	NA

NA, not applicable. Data are expressed as means ± SEM

Examination of epilepsy susceptibility

Mice in both the CFS model group and the control group were raised until 8 weeks of age for subthreshold stimulation with PTZ. An intraperitoneal injection of PTZ at a dosage of 40 mg/kg was administered, after which the mice were placed in a 15 × 15 × 30 cm plastic enclosure and observed for seizure behavior for 30 min. Following this observation period, the mice were euthanized and their brain tissues were carefully extracted for freezing in liquid nitrogen. The severity of seizures was classified and scored as the Racine grading scale. The experimental design and further details are illustrated in (Fig. 1A).

Microvascular isolation and histologic sample Preparation

Referring to the Ogata et al. Method and updated [19], cerebral capillaries were isolated from frozen mouse brains. Briefly, throughout the brain extraction process, we worked quickly on ice (within 1 min) and then immediately underwent liquid nitrogen freezing, followed by transfer to a -80 °C freezer for storage. The frozen brain tissues were thawed and transferred immediately to a 2 mL centrifuge tube (within 1 min), 1 mL of homogenization buffer (100 mM NaCl, 4.6 mM KCl, 2.5 mM $CaCl_2$, 1.2 mM KH_2PO_4, 1.2 mM $MgSO_4$, 15 mM HEPES, pH 7.4) and stainless-steel beads (3.2 mm, 1.8 g; TOMY SEIKO, Tokyo, Japan) were added, then a bead homogenizer was used to homogenize the brain tissues at a rate of 50 Hz for 2 min. The homogenate was transferred to a new 2 mL centrifuge tube and then centrifuged (1000 *g*, 10 min, 4 °C). The supernatant (50 µL) after centrifugation was collected in another tube as the entire brain fraction. The rest of the homogenate was transferred to a new 2 mL centrifuge tube and centrifuged at 1000 *g* for 10 min at 4 °C. The supernatant was carefully removed, and the precipitate was resuspended in 1 mL of homogenization buffer by adding an equal volume of 32% (*w/v*) dextran/homogenization buffer, inverted to mix, and then immediately centrifuged at 4500 *g* for 15 min at 4 °C. Supernatants were collected in a new 2 mL tube, and the precipitate was stored on ice. The supernatant was centrifuged again (4500 *g*, 15 min, 4 °C) and discarded the resulted supernatant. Kimwipe was used to remove the fatty components adhering to the top of the tube wall (capillaries clumped together at the bottom) to prevent lipid contamination from interfering with subsequent capillary endothelial cell extraction and functional analysis. The precipitate was suspended in Suspension Buffer (homogenize buffer containing 25 mM $NaHCO_3$, 10 mM glucose, 1 mM pyruvate, and 5 g/L bovine serum albumin) for 200 µL × 2, and the two suspension samples were combined into one tube. The samples were filtered through a 70-µm cell filter and washed four times with 500 µL of suspension buffer. The combined suspension samples were then added to a cell filter containing

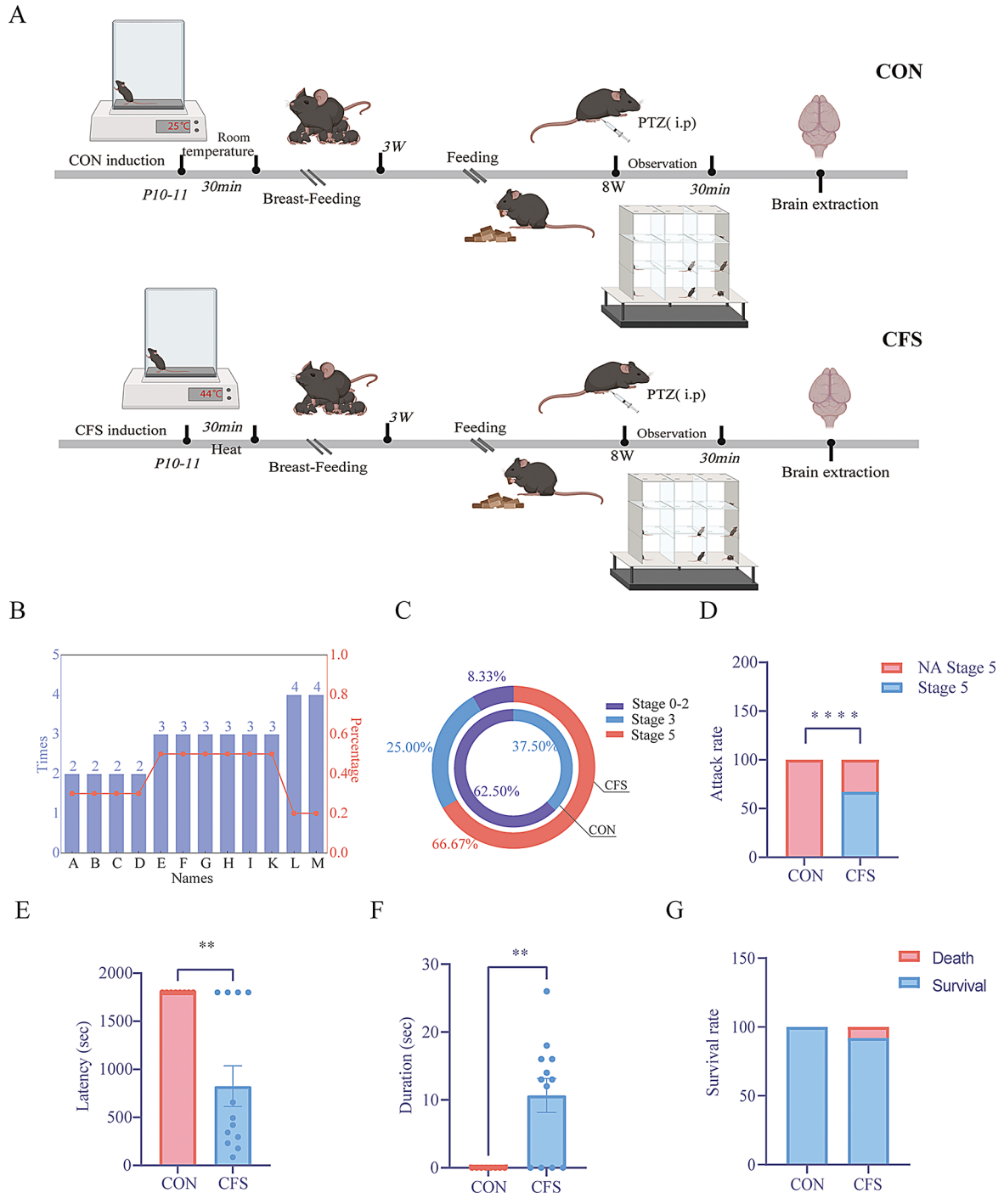

Fig. 1 Hot Air-Induced CFS mice in infantile increases epilepsy susceptibility in adulthood. **A**) Protocol for assessing susceptibility to seizures after adulthood following CFS. **B**) Times and overall distribution of grade V grand mal seizures in hot air-induced CFS mice (left Y-axis represents the number of grand mal seizures, right Y-axis represents the total proportion of such seizures). **C-G**). The severity of seizures was evaluated according to Racine's classification after an 8 W injection of 40 mg/kg PTZ, and the overall proportion of seizure classes, grand mal latency, duration, and mortality were assessed, respectively. Con mice ($n=8$) and CFS mice ($n=12$). (Adapted from BioRender.com (2024). Retrieved from https://app.biorender.com/biorender-templates.)

800 mg of glass beads (0.35–0.5 mm; AS ONE; Osaka, Japan) and washed 10 times with 500 µL of suspension buffer. After washing, the glass beads were transferred to a new tube using a spatula, and 1 mL of suspension buffer was added and mixed inverted. The supernatant was then quickly transferred to a new tube. Another 500 µL of suspension buffer was re-added to the glass microbeads, inverted and mixed, and the supernatant was

quickly transferred to the previous tube and the collection was repeated. Centrifugation (3300 *g*, 5 min, 4 °C) was performed to remove the supernatant, and the pellet was centrifuged again (3300 *g*, 5 min, 4 °C) with BSA-free suspension buffer. The pellet was resuspended in 100 μL of homogenization buffer, and part of the isolated brain capillary fraction was taken for microscopic analysis. The remaining samples of the isolated brain capillary fraction were lysed by ultrasound in lysis solution (50 mM HEPES, pH 7.5; 1% TritonX-100; 0.1% SDS; 500 mM NaCl;10 mM $MgCl_2$;1× protease inhibitor cocktail) [20]. Protein concentrations were determined using the Pierce BCA protein assay kit (PA115, Tiangen, Beijing, China).

Quantitative discovery-based proteomic analysis of mouse brain capillaries

Protein samples were reduced with dithiothreitol (20 mM) for 1 h at 37 °C and then alkylated with iodoacetamide (40 mM) for 45 min in the dark at 25 °C. Six volumes of methanol were added and the proteins were precipitated at -40 °C for at least 4 h. The proteins were then digested in a digestion buffer (50 mM NH_4HCO_3) by adding sequenced grade trypsin (0000547581, Promega, USA) for 16 h at 37 °C at an enzyme/substrate ratio of 1:20 (*w/w*). The reaction was terminated by the addition of 2% trifluoroacetic acid. The digested peptides were desalted using a C_{18} solid phase extraction (SPE) cartridge based on reference [21]. The eluted peptides were vacuum dried in a lyophilizer and stored at − 40 °C for use.

The desalted peptide samples were redissolved with 10 μL 0.1% FA-water solution containing the standard peptides and centrifugated at 15,000 *g* for 5 min. The supernatant was taken to the injection vial, followed by placing it in the 7 °C injection tray of the nanoscale liquid chromatograph. Samples were analyzed by Orbitrap Fusion Tribrid mass spectrometry (Thermo Scientific, USA) coupled with Vanquish Neo UHPLC System (Thermo Scientific, USA). The samples were uploaded onto a C18 column (20 cm × 75 μm id, 3 μm) and separated at a flow rate of 300 nL/min. In this study, we used 0.1% formic acid aqueous solution and acetonitrile containing 0.1% formic acid as solvent A and solvent B, respectively. The gradient of samples totaled 135 min: 2–5% solvent B in 2 min, 5–24% solvent B in 92 min, followed by an increase to 35% B in 20 min, 35–95% solvent B in 10 min, and 95–100% solvent B in 5 min.

The MS parameters for sample analysis were: (1) Ion source type = ESI; Ion source tube temperature = 300 °C; Positive ions = 1800 V; (2) MS: Scanning range (m/z) = 350–2000; Resolution: 60,000; Maximum injection time: 50 ms; Automatic gain Control: 4e5. MS^2 scanning parameters: resolution: 30,000; maximum injection time: 100 ms; automatic gain control: 1e5; high energy fragmentation (HCD): 35%.

Proteomics and bioinformatics analysis

All proteomic raw data files were retrieved using DIA-NN software based on reviewed mouse database from UniProt (https://www.uniprot.org/). Two missed cleavage sites were allowed to be used with cysteine aminomethylation, N-methionine excision, N-terminal acetylation, and oxidative setup as modifications. The peptide length ranges from 7 to 30 amino acids, the precursor charge ranges from 1 to 4, and the precursor m/z ranges from 300 to 1800. A default false discovery rate threshold of 1% was used at the peptide and protein levels. To investigate differences in proteomic features, partial least squares discriminant analysis (PLS-DA) was employed. Differentially expressed proteins (DEPs) were analyzed to identify significantly down- or upregulated proteins according to the criteria of fold difference ≥ 2 and a significance level of $P < 0.05$ using Volcano plot analysis. The DEPs between CFS and control mice were analyzed by keyword search using Gene card 5.20 (www.genecards.org) to identify the list of relevant proteins; the protein-protein interaction network analysis were conducted by STRING 12.0 (https://string-db.org/) and visualized by Cytoscape 3.7.2; followed by the Kyoto Encyclopedia of Genes and Genomes (KEGG) and Gene ontology (GO) signaling pathway enrichment analysis and visualization of proteins using STRING 12.0. Gene set enrichment analysis 4.3.2 (GSEA) (www.gsea-msigdb.org/gsea/index.jsp) was conducted on the entire protein set to calculate gene set enrichment scores in functional pathways.

Western blot analysis

Except for the mice used for vascular isolation, other individual mouse brain cortex protein samples were performed (CON = 3, CFS = 3), and total proteins were extracted with RIPA lysis buffer (China Report) containing protease and phosphatase inhibitors. Protein concentration was determined by BCA kit (PA115, Tiangen, Beijing, China). Extracts (20 μg protein) were separated by 10–12% SDS-PAGE gels and subsequently transferred to PVDF membranes (Merck Millipore, MA, USA), which were then closed with 5% BSA (S7425, Solarbio, Beijing, China) for 2 h at room temperature. The membranes were incubated with primary antibodies against Occludin (1:1000, #GB111401, Servicebio, Wuhan, China), Aqp4 (1:1000, #WL02267, Wanleibio, Beijing, China), and β-actin (1:1000, #GB15003, Servicebio, Wuhan, China) at 4 °C overnight. Next, they were incubated with horseradish peroxidase-conjugated secondary antibodies for 1 h at room temperature and washed again with TBST. Protein bands were visualized by Dual color infrared fluorescence imaging system (9260, Odyssey,

USA). The protein results were analyzed and quantified using Image J software (version 2.0.0, USA).

RNA extraction and qRT-PCR analysis

The total RNA of the brain tissues was extracted using the RNA extraction kit (RR047A, Takara, Beijing, China) according to the manufacturer's protocol. A total of 1 μg of RNA was reversely transcribed into cDNA using the iScript cDNA synthesis kit. The qRT-PCR analysis was performed using SYBR Green Master Mix on the CFX48 Real-Time PCR system from Illumina (ECO, Illumina, USA). GAPDH was used as a housekeeping gene. Relative mRNA expression was calculated using the 2-ΔΔCT method. The sequences for the primers used are listed in Supplementary (Table S4).

Immunofluorescence staining

After anesthetized deeply, mice were transcardially perfused with ice-cold PBS followed by 4% paraformaldehyde to fix the brains. Brains were then removed and sequentially immersed in 4% paraformaldehyde, 30% sucrose to facilitate fixation and dehydration. Coronal brain sections with a thickness of 25-μm were sliced using the freezing microtome (CM1680; Leica, Hessen, Germany). After washing with PBS and PBS + 0.3% Triton, brain sections were blocked with 10% g fetal calf serum for 1 h. Subsequently, the brain sections were incubated overnight at 4 °C with the following primary antibodies: anti-Occludin (1:1000, #GB111401, Servicebio, Wuhan, China). After washing, Alexa Fluor 488 Conjugated Antibody was applied. Following this, nuclear staining was performed using DAPI (0100 – 20, SouthernBiotech, USA). Ultimately, the images were observed using Pannoramic Slide Scanners (Pannoramic SCAN; 3D HISTECH, Hungary), and the quantification process was quantified using Image J software (version 2.0.0, USA).

TEM

After perfusion, the one mm3 fragments of the mouse cerebral cortex were fixed in 4% glutaraldehyde at 4 °C overnight, followed by dehydration and embedding. Imaging was performed on 70 nm ultra-thin sections counterstained with uranyl acetate and lead citrate by a HT7800/HT7700 transmission electron microscope (Hhitachi). Random microvessel areas from the brain tissue of each mouse were oriented for vesicular density quantification analysis.

Tissue metabolites imaging by AFADESI-MSI

Custom-built AFADESI-MSI platform (Prosolia Omni-Spray 2D, Viktor, China) equipped with Orbitrap Fusion mass spectrometer (Thermo Scientific, USA) and AFADESI ion source was used for tissue metabolites imaging. The experiment was carried out in both positive and negative ion modes at *m/z* 100–1000 Da. The spray solvent used in this study was acetonitrile and water (80:20, *v*/*v*), and the flow rate of spray solvent was set to 5.0 μL/min. Sprayer voltages were set at 4500 V and – 4500 V in positive and negative ion mode, respectively. The extracting gas flow of AFADESI ion source was 12 L/min. The flow rate of nebulizing gas (N_2) was set to 0.6 MPa. Imaging analysis was performed by continuously scanning the tissue section in *x*-direction at 150 μm/sec, separated by a 100 μm vertical step in *y*-direction. MassImager Pro™ software was used for background subtraction, image reconstruction, and the calculation of average metabolite expressions in region of interest [22].

All tissue samples were stored at -80 °C before sectioning. Tissue sections were performed at 20 °C using a cryotome (CM1680; Leica, Hessen, Germany). Brain tissue sections (sagittal) were cut to 12-μm thick and subsequently fixed on precooled Fisher slides (12-550-15, Thermo, Bremen, Germany). After sectioning was completed, the slides were stored at -80 °C and transferred cryogenically to a desiccator at -20 °C for drying two hours prior to analysis to avoid condensation effects associated with – 80 °C storage of the slides.

Assessment of BBB permeability

The fluorescent tracer Evans Blue (EB) (B0001-7, Red-Party Tech, USA) was injected through the tail vein at a dose of 2% EB (4 ml/kg) before euthanized. Brain sagittal Sect. (12 μm thick) were used to observe tracer leakage through the damaged BBB. Data reading, ion image reconstruction, and background deduction were performed via the MassImager 1.0 Mass Spectrometry Imaging System workstation. Spectra of average mass regions were obtained by overlaying optical images, selecting neighboring tissue sections in the region of interest and mass spectrometry imaging.

Surgical procedures

The anesthesia protocol involved the use of isoflurane (3% for induction, 1.2–1.5% for maintenance) for the procedure. Subsequently, the mice were immobilized in a mouse-adapted stereotaxic frame. To prevent eye damage, erythromycin ophthalmic ointment was applied. A sagittal incision was made in the scalp to access the fontanelle for positioning the cranial mounting trocars and screws. Body temperature maintenance within the normal physiological range was ensured by utilizing a heating plate throughout the procedure to safeguard the mice's health. The implantation included EEG electrodes and guide cannulae for facilitating intracerebroventricular (i.c.v.) injections. The trocar was placed on the dura mater with the following coordinates of the bregma: anteroposterior (AP), – 0.82 mm; lateral (ML),

± 1.3 mm; depth (DV), -2 mm, and, to prevent clogging during the recovery period, a double needle was inserted and secured with a dust cap. The recording electrode was mounted anterior to the trocar and the electrode and trocar were secured with dental adhesive. After awakening from surgery, the mice were placed in an open animal cage and allowed to move freely. Subsequent experiments were performed 1 week after surgery.

The mouse electrodes were connected to the lead socket of the rotary commutator and then linked to the PowerLab amplification system to obtain baseline recordings. Incyclinide (5 μm) was microinjected into each lateral ventricle at a rate of 10 nL/min for a total volume of 3ul per ventricle, over a period of 10 min. Following the injection, the micropipette was left in place for 5 min before being slowly withdrawn. Subsequently, a sub-threshold dose of PTZ (40 mg/kg) was administered via intraperitoneal injection to the mice. Thirty minutes after PTZ administration, seizure activity in the mice was evaluated using EEG and behavioral measures.

Behavioral and EEG analysis

Mouse EEG data were analyzed and quantified using LabChart Pro V8.1.13 software (AD Instruments, Australia). Data were digitized at 1000 Hz and filtered (EEG, 0.5–45 Hz) for further analysis. EEG power spectra were categorized into δ (0.5 ~ 4 Hz), θ (4–8 Hz), α (8–15 Hz), and β (16–35 Hz) according to the different frequency bands. PTZ-induced seizures were defined as high-amplitude (> 2 baseline) high-frequency (> 5 Hz) multi-spike discharges lasting > 5 s. Epileptic behaviors were similarly rated using an adaptive Racine scale. Behaviors were scored by observers who were unaware of the treatment. The highest score was recorded every 5 min for 30 min after PTZ.

Statistical analysis

All data are expressed as mean ± standard error (SEM) unless otherwise stated. GraphPad Prism 9.5.1 (GraphPad Software, San Diego, USA) for Windows was used for statistical analysis. Unpaired Student's t-test and nonparametric tests were used to compare differences between the two groups, $P < 0.05$ was considered statistically significant.

Results

CFS exposure in infancy increases epilepsy susceptibility in adulthood

To assess the impact of CFS experienced in infancy on their vulnerability to developing epilepsy in adulthood, a hot air-induced CFS mice model was utilized (Fig. 1A). In this model, hot air was used to induce FS in 10-11-day-old mice (P10-11) as previously described [5], while the severity of seizures was assessed using the Racine scale. Mice with grade V and above seizures twice were defined as successful CFS modeling (Fig. 1B). Thereafter, the mice were observed daily for 2 h at consistent intervals and did not display any noticeable signs of epileptic behavior.

The mice in each group showed similar body weights, indicating the modeling method didn't affect their later-life growth (Fig. S1). With 40 mg/kg PTZ, control mice had grade III seizures in 37.50% ($n = 3$) of cases and no seizures in 62.50% ($n = 5$, Fig. 1C ~ D). CFS model mice had grade V; seizures in 66.7% ($n = 8$), grade III in 25.00% ($n = 3$), and no significant seizures in 8.33% ($n = 1$) of cases (Fig. 1C ~ D). It is indicating that mice who had experienced CFS during infancy exhibited significantly greater seizure severity and maximum seizure grade in adulthood. The latency and duration of grade V seizures were significantly shorter and longer, respectively, in the CFS mice compared to the control ($P < 0.01$); while the mortality rate associated with the induction of epileptic susceptibility in adulthood was not statistically significant (Fig. 1E ~ G). Therefore, CFS exposure in infantile mice increases epilepsy susceptibility in adulthood.

Characterization of BBB-associated proteins in cerebral capillary sites

The expression levels of proteins in isolated brain capillaries were quantified using DIA-based proteomics. Proteomics data revealed that proteins unique to brain capillary endothelial cells were found in highest abundance within isolated brain capillaries. In contrast, proteins that are specifically expressed by astrocytes, microglia, neurons, and oligodendrocytes were found to be less common in these isolated capillaries [23], but they were still identified in our experiment (Fig. 2A).

Taking the control group as an example, we analyzed the amounts of brain cell marker proteins in both the isolated brain capillary fraction and whole brain fraction (Table S1). Compared to the whole brain fraction, the levels of synaptophysin (syp, the marker for neurons) and corona-1a (coro1a, microglia) in the brain capillary fraction decreased by 77.8% and 30.1%, respectively. Conversely, Mdr1a, the brain capillary endothelial cell marker, increased 60.8-fold in the isolated fraction (Fig. 2B ~ C). The number of astrocyte and pericyte marker proteins was significantly elevated in the cerebral capillary fraction compared to the whole brain ($P<0.05$, Fig. 2D). Astrocytes and pericytes consistently adhering to the brain capillary endothelial cell and therefore, enriched with brain capillaries in our method. The above results confirmed that the isolated capillaries method is suitable for BBB proteomic studies, as reported in [19].

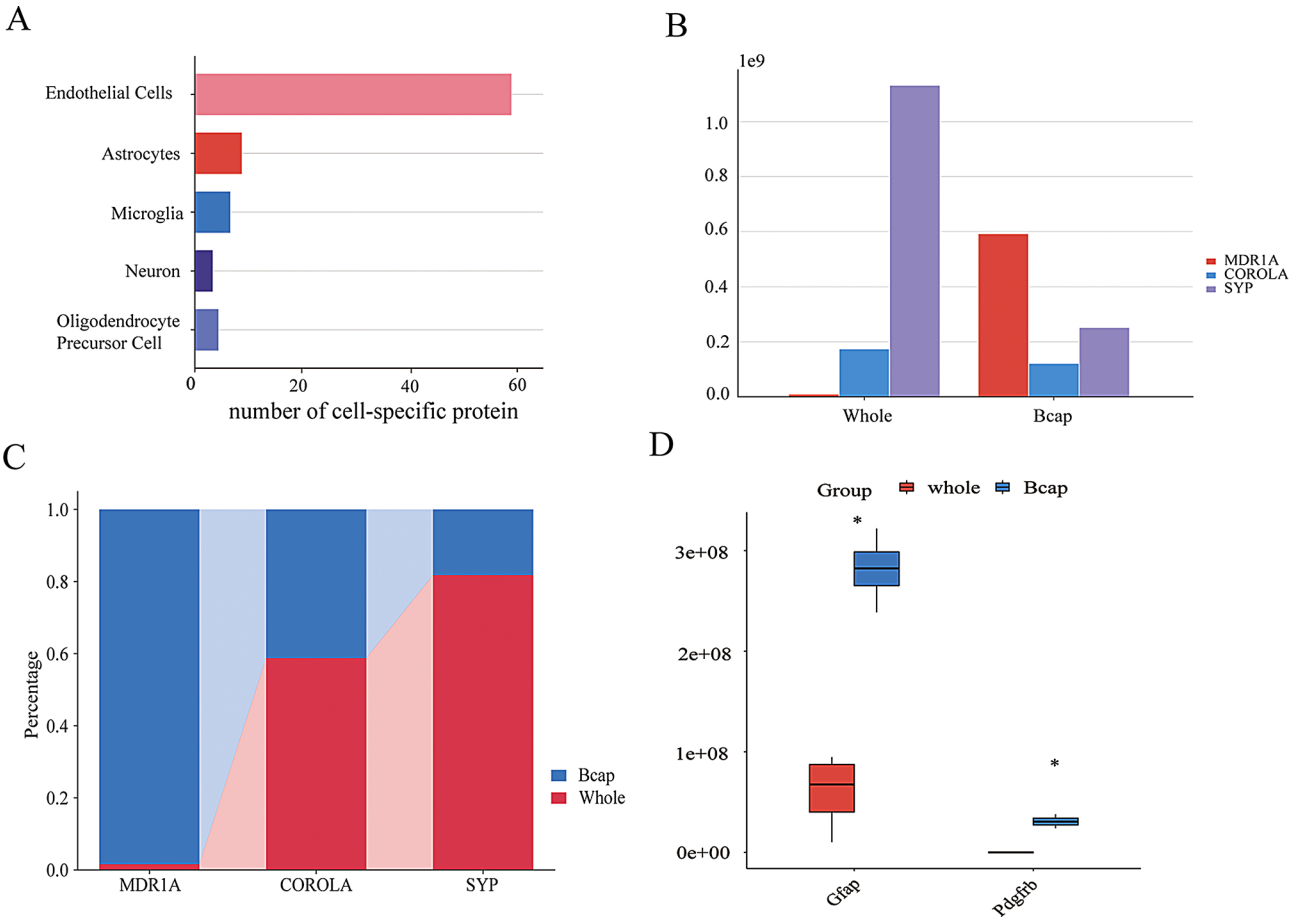

Fig. 2 Enrichment and characterization of blood-brain barrier-associated proteins in cerebral capillary fraction. **A**) Number of cell-specific proteins quantified by proteomic analysis (Proteins selectively expressed in each cell type were extracted and selected according to the criteria that the mRNA expression ratio (fragments per kilobase of exon per million mapped fragments [FPKM] value in most highly expressed cell types/FPKM value in the second highly expressed cell types) was over 10-fold [19]. **B-C**) Amount and ratio of marker proteins between isolated capillary and whole brain fractions of the brain. **D**) Amounts of astrocyte and pericyte marker proteins in isolated capillary fractions and whole brain fractions

Changes of protein expression in isolated brain capillaries of CFS mice

To investigate the BBB proteomic changes of epilepsy susceptibility of mice, brain capillaries were isolated from the brains of CFS and CON mice (Fig. 3A). It is clearly shown that most brain tissues were removed (Fig. 3A), indicating high purity of capillary fragments. Moreover, the levels of the protein in cerebral capillaries isolated lysates from CFS mice did not significantly differ from those isolated lysates from litter-matched control mice (Fig. 3B). This indicates that experiencing CFS in infancy does not induce substantial changes in vascular morphology and protein expression overall.

The proteomic profiles of brain capillaries (5674 proteins) from CON mice ($n = 4$) and CFS mice ($n = 3$) were analyzed using PLS-DA, generating score plots (Fig. 4A). The plots and ellipses (95% confidence intervals) demonstrated clear separation between cerebral capillaries in CFS and CON groups, with PC1 explaining 91.41% of variance. The above results suggest that mice that experience CFS in infancy alter the proteomic profile of the BBB.

A total of 365 DEPs were identified as shown with volcano plot, of which 189 proteins were significantly down-regulated and 175 proteins were significantly up-regulated (Fig. 4B). There are 2371 "blood-brain barrier" related proteins in GeneCard database. Taking the 2371 proteins as background library, it is easy to identify 53 BBB-related DEPs (49 down-regulated, 4 up-regulated; Table S2, Fig. 4C ~ D). A more comprehensive analysis of the 53 BBB-related DEPs revealed that the DEPs involved in BBB permeability, disruption, integrity, and physiological function were mostly down-regulated, meanwhile the DEPs involved in BBB leakage and damage were all down-regulated (Fig. 4E). Therefore, the results suggested that the 53 BBB-related proteins may be related to the epilepsy susceptibility of CFS mice.

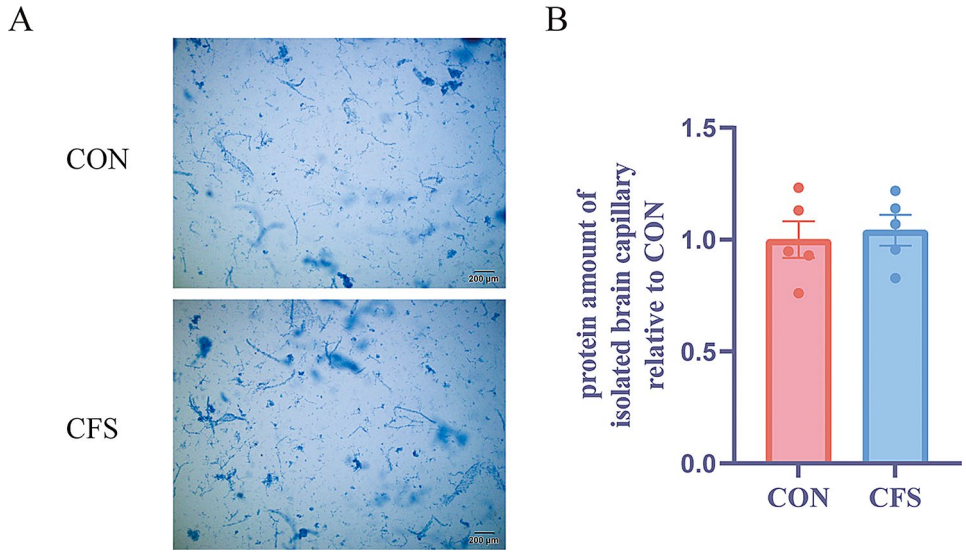

Fig. 3 Isolation of brain capillaries in adult CFS mice. **A**) Images of isolated brain capillaries from CON and CFS mice. The capillaries were stained with trypan blue. Scale bar = 200 μm. **B**) Protein levels in isolated brain capillaries of CON and CFS mice. The amount of protein was normalized to brain weight. Bars represent the mean ± SD values ($n = 5$). Plotted points represent individual values

ECM-receptor and integrin signaling pathways related with epilepsy susceptibility

To determine the altered biological function of the BBB, we performed enrichment analysis of the KEGG pathway in 365 cases of DEPs in CFS mice, among which 9 pathways were significantly enriched ($P < 0.05$), including the spliceosome, ECM receptor interaction, and arrhythmogenic right ventricular cardiomyopathy (Fig. 5A). To further explore the biological functions associated with the 53 DEPs related to the BBB, we conducted KEGG annotation on these DEPs. Our analysis revealed that the ECM-receptor interaction signaling pathway was the most significant (Fig. 5B). This finding indicates that the pathway most critically involved in the alteration of the BBB in CFS mice is indeed the ECM-receptor interaction. We additionally conducted pathway re-annotation on the enriched pathways using the ClueGo-plugin. The ECM-receptor interaction was found as the core pathway. 5 genes (Itgb4, Itga8, Itga10, Col4a5 and Col4a6) were significantly enriched in ECM-receptor interactions (Fig. 5C). Next, in order to determine more biological functions of the above genes, we similarly performed GO annotation analysis by STRING, and notably the significantly enriched GO terms integrin-mediated signaling pathways associated with biological processes (BPs) were five DEPs (Ctnna1, Nrp1, Itga10, Itgb4, and Itga8 (Fig. 5D ~ E). Specifically, Itga10, Itgb4, and Itga8 were also significantly enriched in the ECM-receptor interaction pathway (Fig. 5C). The results indicate a dysfunction in integrins and cell matrix adhesion, suggesting that the abnormal expression of these genes may be associated with the pathogenesis of epilepsy susceptibility.

Besides, GSEA pathway analysis of the 5,674 identified proteins found that ECM-receptor interaction and integrin-mediated signaling pathways were significantly enrichment ($P < 0.01$, FDR < 0.05; Fig. 5F ~ G). Notably, Col4a5, Col4a6, Itgb4, Itga6, and Itga8, which are core genes in these pathways, were markedly downregulated, suggesting dysregulation of integrin- and ECM-related biological processes (Fig. S2). These findings are consistent with the GO and KEGG enrichment analyses performed using DEPs, underscoring the critical role of ECM-receptor interaction and integrin-mediated signaling pathways in the pathogenesis and progression of epilepsy susceptibility.

The protein-protein interactions among DEPs were analyzed using the STRING online platform, and a small network was visualized with Cytoscape (Fig. 6A). Each node represented a protein. The proteins in the network were ranked according to their network degree values. The top 10 proteins in descending order were Cldn5, Itgb4, Itga8, Aqp4, Itga10, Col4a5, Col4a6, Col14a1, Ocln, and Slc38a3. The expression levels of these proteins in the CFS group were all down-regulated compared to the control group (Fig. 6B ~ C). Interestingly, Itgb4, Itga8, Itga10, Col4a5, and Col4a6 are DEPs enriched to the ECM-receptor interaction pathway and integrin-mediated related pathway (Fig. 5B ~ C). The fold changes in the levels of proteins related to the top five KEGG pathways and biological processes were examined to determine their upregulation or downregulation. "ECM-receptor interaction" (median: -1.77-fold), "GABAergic synapse" (median: -1.53-fold), "Focal adhesion" (median: -1.77-fold) and "integrin-mediated signaling pathway" (median: -1.07-fold) were estimated to be downregulated

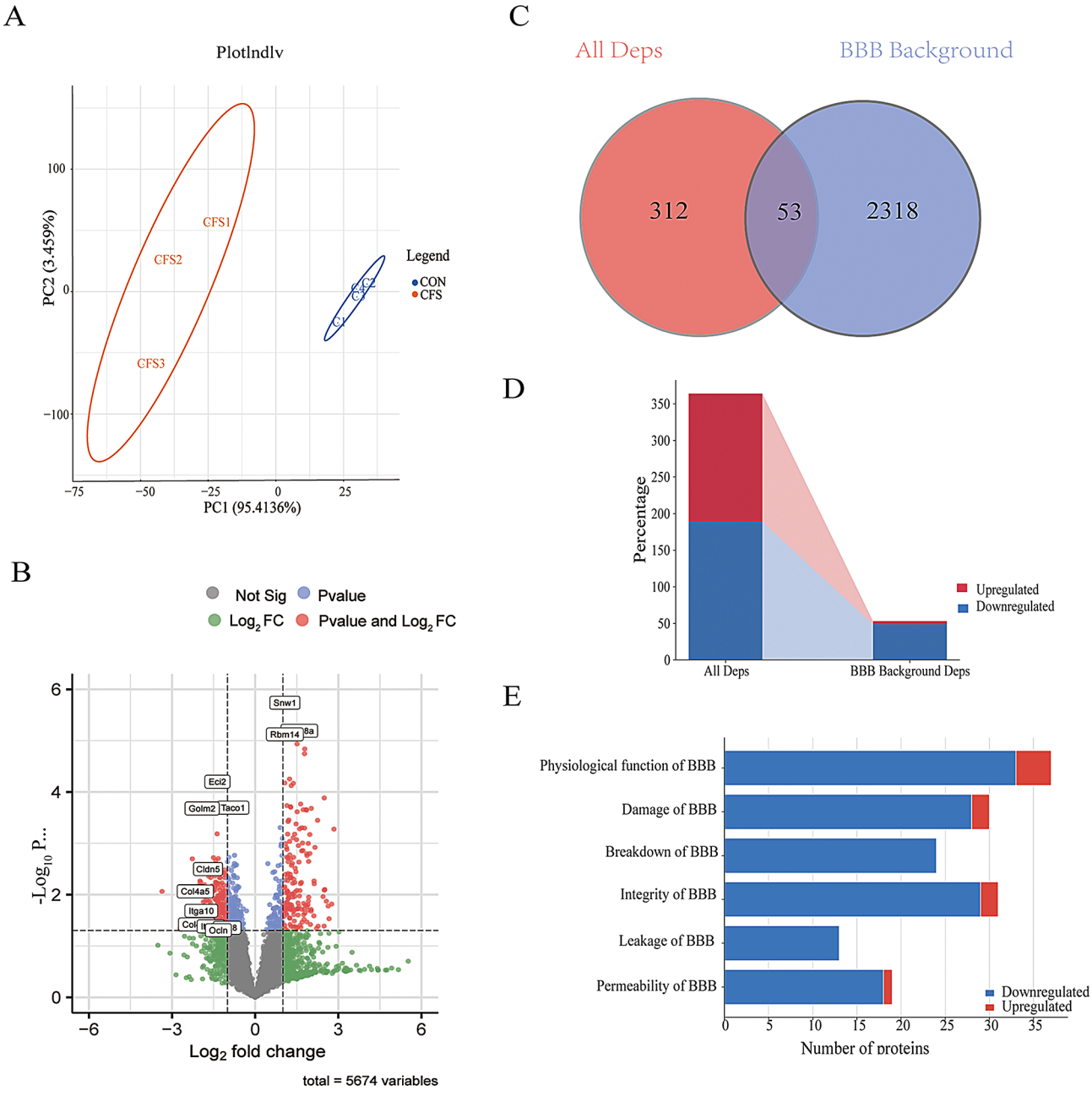

Fig. 4 Proteomic analysis of identified proteins and BBB-associated proteins in brain capillaries of CFS mice. **A**) PLS-DA for the identification of proteins in isolated brain capillaries. **B**) Volcano plots of proteins identified in isolated brain capillaries (red dots indicate Log2FC ≥ 1, $P < 0.05$; blue dots indicate Log2FC≤-1, $P < 0.05$). **C**) Venn diagram of isolated brain capillaries identifying proteins and proteins in the context of the BBB (365 proteins were identified in isolated brain capillaries (red circle), 2371 proteins were identified in BBB background (blue circle), and 53 proteins were identified). **D**) Up- and down-regulation of isolated brain capillary differential proteins in the context of the BBB (Their folding changes are shown in Table S2). **E**) More detailed bioinformatic analysis shows the number of proteins involved in the pathophysiology of BBB (Protein names and their fold change are listed in Table S3). CON mice ($n = 4$) and CFS mice ($n = 3$)

(Fig. 6D ~ E). Ocln and Aqp4 are essential proteins involved in maintaining the integrity and function of the BBB. We verified the alterations in their protein expression using Western Blot method (Fig. 6F), which were consistent with our proteomic data findings.

mRNA expression data supported the proteomic findings

DEPs associated with the ECM-receptor interaction pathway were significantly downregulated, as illustrated in the heatmap (Fig. 7A). Integrins, composed of α and β subunits, function as transmembrane receptors that bind to the ECM extracellularly and to the cytoskeleton

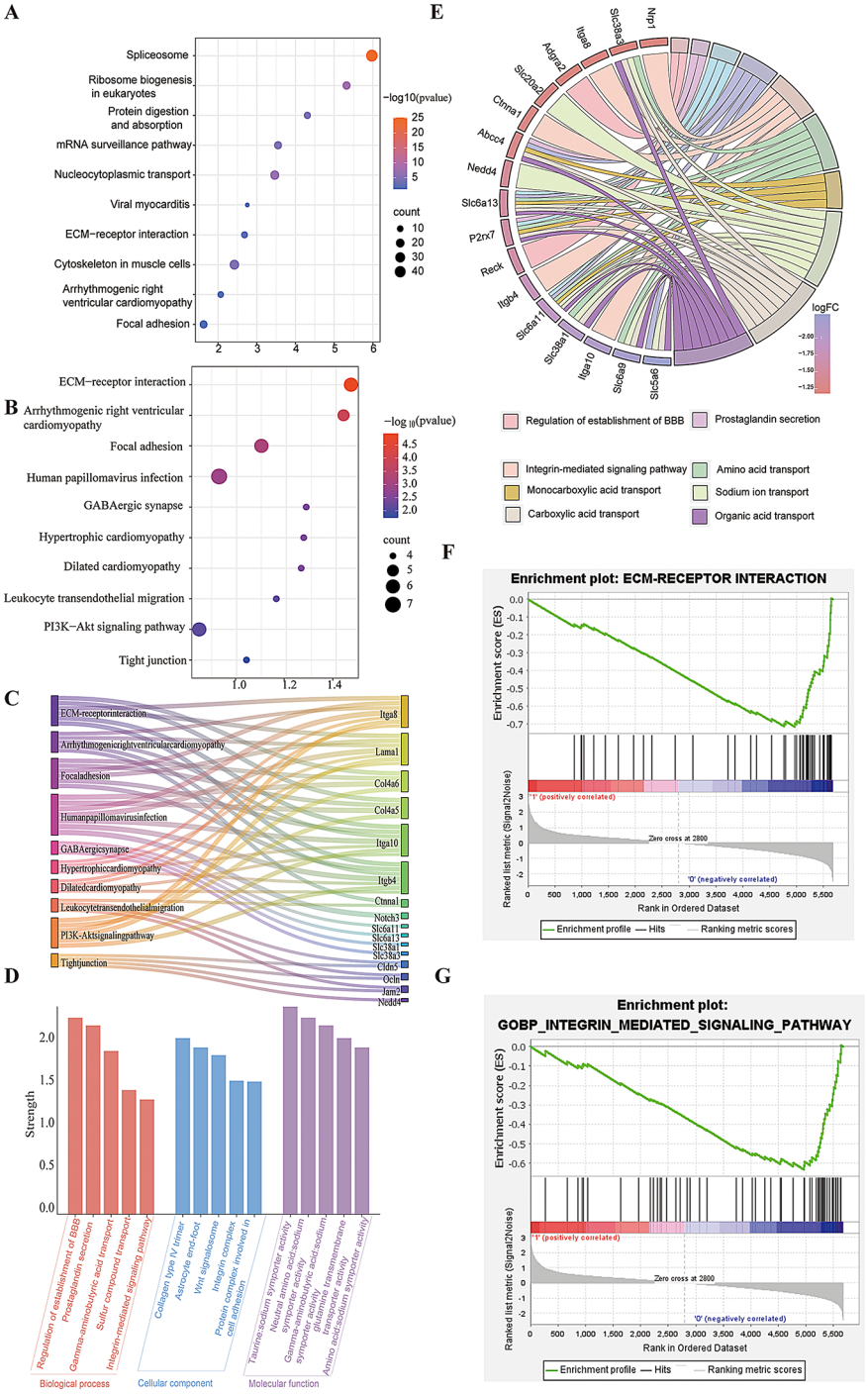

Fig. 5 Bioinformatics analysis of Deps and GSEA in CFS mice. **A**) Bubble plot of KEGG pathway enrichment in isolated brain capillary DEPs. (x-axis represents the strength factor, with larger values indicating a larger proportion of DEPs annotated to the pathway. y-axis represents KEGG pathway annotation entries. Dot size indicates the number of DEPs annotated to pathway. Dot color indicates that the enriched KEGG pathway ($-\log_{10}$*P*-value) is statistically significant, with blue being the lowest and red the highest). **B**) Bubble plot of KEGG pathway enrichment of 53 DEPs associated with BBB. **C**) DEPs enriched in the top ten KEGG pathway. **D**) Enrichments of the first 5 biological processes, cellular components, and molecular functions. **E**) DEPs enriched in the top ten GO bioprocess pathways. **F**, **G**) GSEA enriched to the pathway integrin-mediated signaling pathway and ECM-receptor interaction

intracellularly. They transduce signals to regulate cell adhesion, migration, proliferation, differentiation, and the remodeling of the ECM [24]. Interestingly, integrin family members ITGB4, ITGA8, and ITGA10, and the key proteins in ECM-receptor interaction pathway including collagen family members COL4A5 and COL4A6, were all significantly downregulated (Fig. 7A). Then, we quantified the mRNA expression levels of these genes

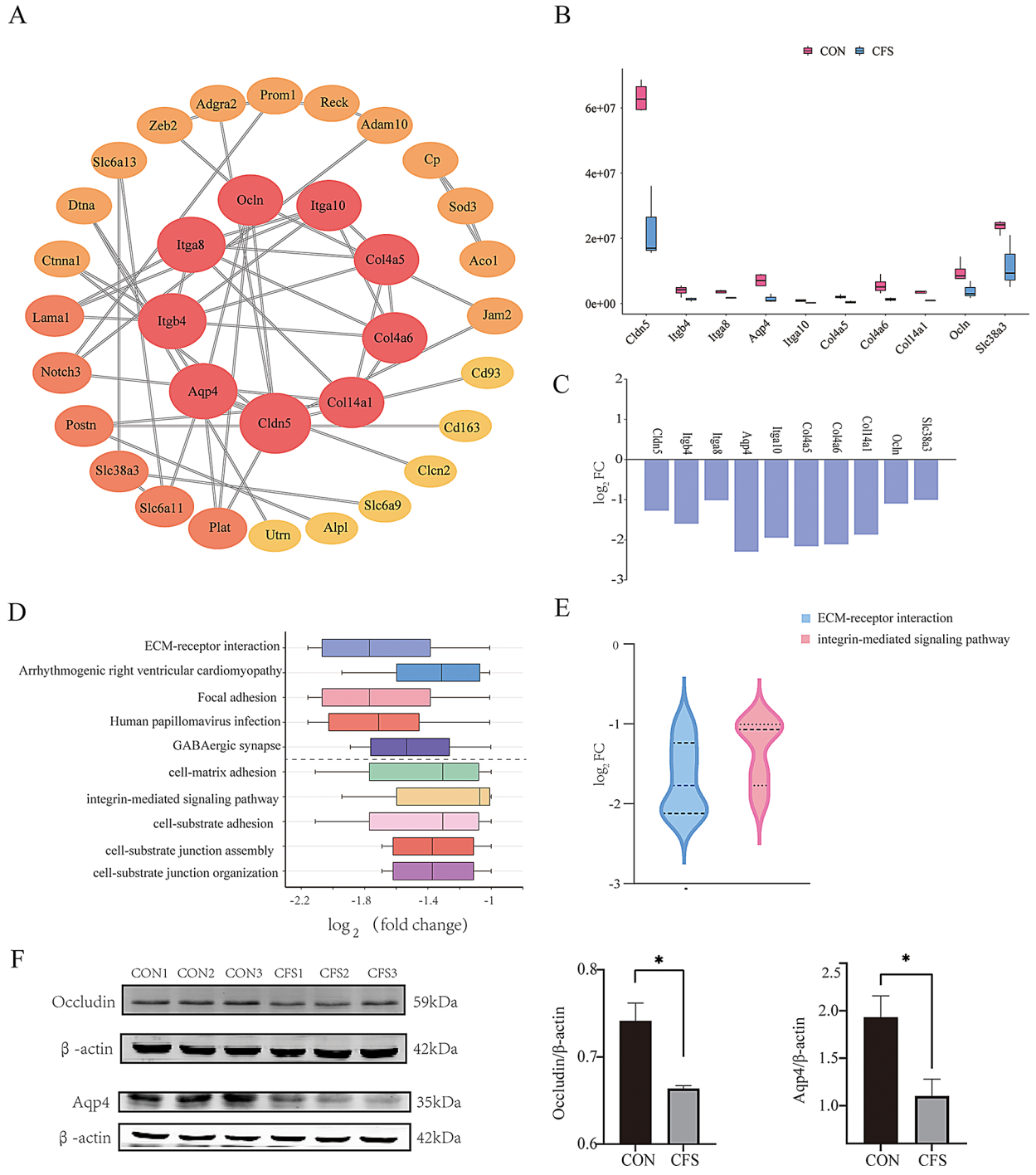

Fig. 6 Changes in biological functions based on differentially expressed proteins in the brain capillaries of CFS mice. **A**) PPI network of isolated brain capillary DEPs in the context of the isolated BBB. (Circles represent genes and lines represent interactions between gene-encoded proteins, The nodes in the network are ranked from highest to lowest based on network characteristics with Degree algorithm. The size and color of the dots indicate the importance of this gene, with yellow being the lowest and red being the highest. PPI, protein–protein interaction). **B, C**) Expression and differential multiplicity of the first 10 central genes in isolated brain capillaries of CFS mice. **D**) Expression changes of relevant differentially expressed proteins enriched in the first five KEGG pathways and GO term. **E**) Changes in the expression of ECM-receptor interaction and integrin-mediated signaling pathway in isolated brain capillaries of CFS mice. Violin plot elements: center line, median; upper and lower lines, upper and lower quartiles. **F**) Western blotting and quantification analysis of Occludin and Aqp4 protein expression in brain tissue ($n = 3$)

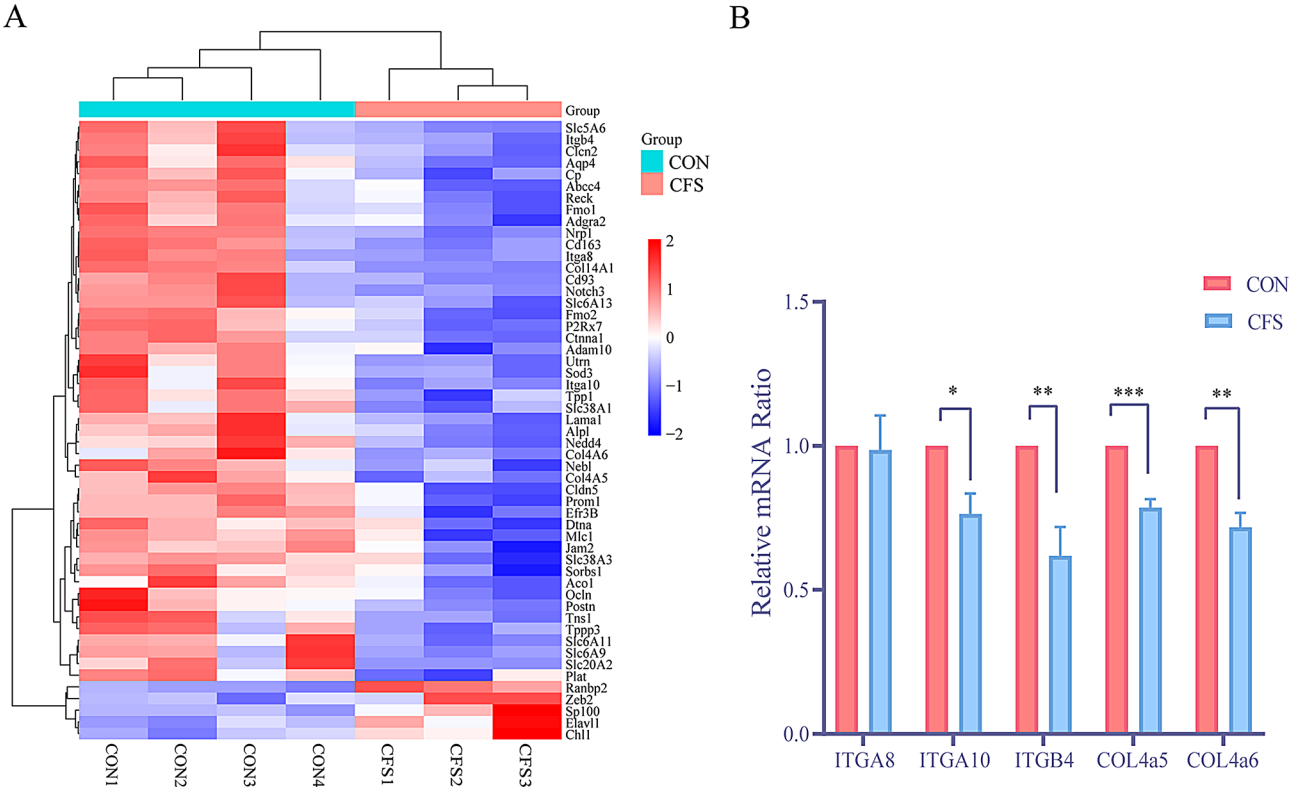

Fig. 7 Alterations in BBB and ECM-receptor interaction-related proteins in CFS mice. **A**) BBB-associated DEPs heat maps of mice in control group ($n=4$) and CFS group ($n=3$). **B**) Validation of selected ECM-receptor interaction-associated DEGs by qRT-PCR ($n=3$)

using qRT-PCR, and the results were consistent with the proteomics results (Fig. 7B). Consequently, the mRNA expression data supported the proteomic findings.

ECM-receptor interaction pathway dysregulation not associated with PTZ treatment

To further support our findings, additional mice (Without-PTZ groups) experienced CFS during infancy, and their BBB proteomic alterations were observed 8 weeks later (Fig. 8A). The proteins related to the ECM-receptor interaction pathway are depicted in (Fig. 8B); both the protein and mRNA the expression levels of key proteins, including ITGB4, COL4a1, COL4a2, HSPG2, and ITGB1, were down-regulated (Fig. 8C ~ D). This downregulation was consistent with the results observed in PTZ treatment mice (Fig. 8C ~ D). Therefore, the ECM function was dysregulated when the mouse experienced CFS during infancy with or without PTZ treatment.

CFS increased the degradation of BBB TJs and basement membrane in C57 mice

We assessed the structural and functional integrity of the BBB in both CFS and CON groups of pups and adult mice using immunofluorescence staining for occludin, as well as tracer EB and transmission electron microscopy. Immunofluorescence staining revealed a significant decrease in occludin fluorescence intensity in the brain tissues of CFS pups (P11) compared to the control group ($p<0.05$). Although a similar trend was observed in adult mice (8 W), the difference did not reach statistical significance (Fig. 9A and C). Functional assessment of the BBB using EB tracer injection demonstrated significantly increased EB leakage in CFS pups (P11) compared to CON pups ($p<0.05$, Fig. 9B and D). This increase in EB leakage persisted in adult CFS mice (8 W), remaining significantly higher than that in CON mice ($p<0.05$, Fig. 9B and D).

Transmission electron microscopy analysis further supported these findings. In control pups (P11), astrocyte footplates exhibited low local density, uniform thickness, and continuous basement membranes, with well-defined and abundant tight junctions (TJs). In contrast, CFS pups (P11) showed extensive edema in astrocyte footplates, along with thinner and less distinct basement membranes, as well as shorter and less defined TJs (Fig. 9E). Similarly, in adult control mice (8 W), the basement membranes were uniformly thick and well-structured, with abundant and tightly packed TJs. However, adult CFS mice (8 W) displayed blurred and slightly fractured basement membranes, fewer TJs, and slightly wider gaps between them (Fig. 9E). These results collectively indicate that BBB structural and functional

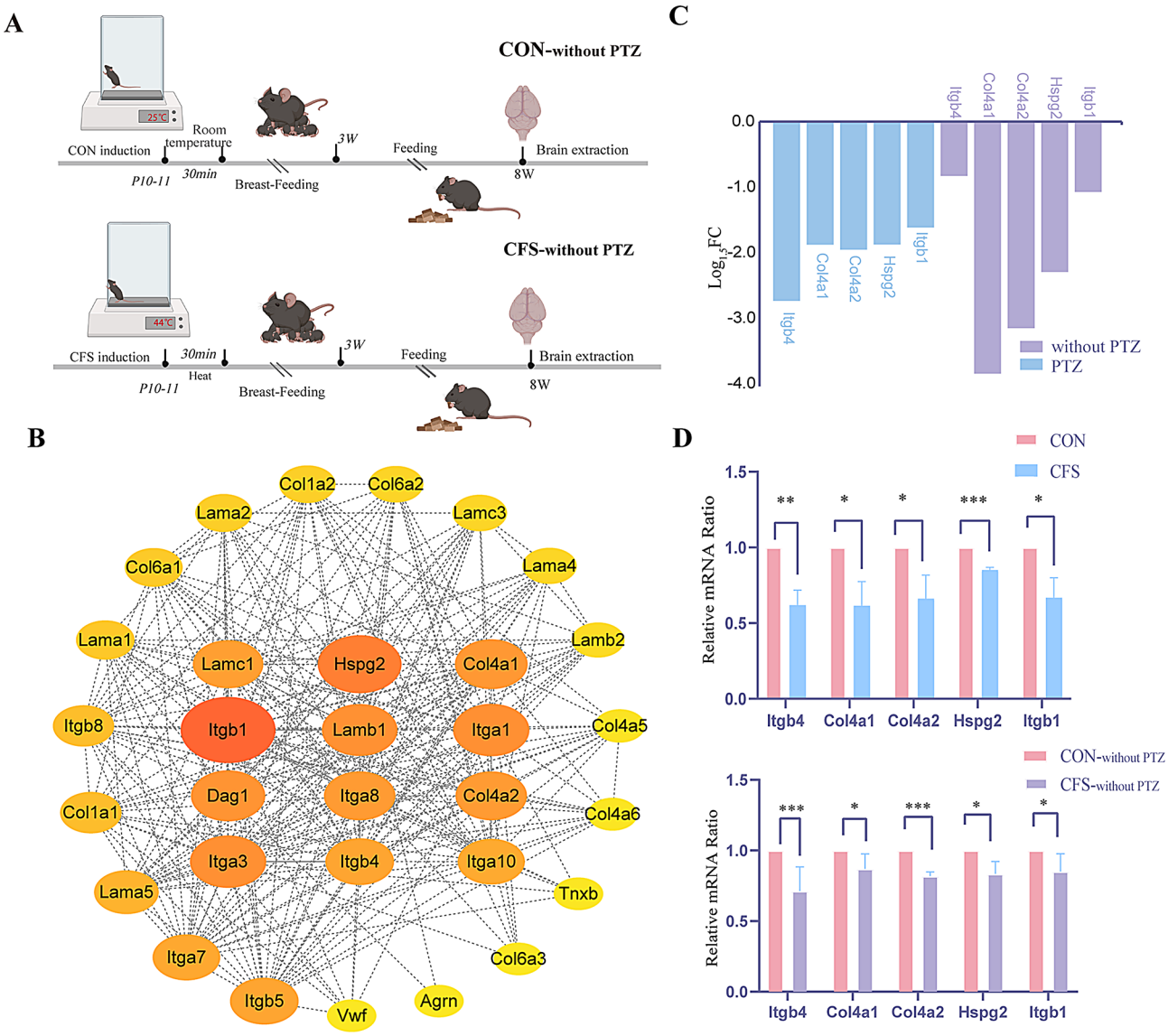

Fig. 8 Further validation that infancy CFS affects ECM functioning. **A)** Hot Air-Induced mouse model of infantile CFS without intervention of epilepsy sensitizers. **B)** PPI networks constructed by core proteins in the ECM-receptor interaction pathway. (Circles represent genes and lines represent interactions between gene-encoded proteins, The nodes in the network are ranked from highest to lowest based on network characteristics with Degree algorithm. The size and color of the dots indicate the importance of this gene, with yellow being the lowest and red being the highest. PPI, protein–protein interaction). **C)** Differential expression of core proteins associated with the ECM-receptor interaction pathway (with or without PTZ) ($n=3$). **D**) Validation of selected ECM-receptor interaction-associated DEGs by qRT-PCR ($n=3$)

integrity is significantly disrupted in CFS mouse pups compared to controls. Although some degree of recovery was observed during growth, BBB impairment persisted in adult CFS mice.

Altered neuroexcitatory metabolites following BBB destruction

To examine whether brain metabolites change during BBB dysfunction, we utilized mass spectrometry imaging (MSI) to determine the distribution of metabolites in various brain regions [25, 26]. MSI has revealed significant increases in the intracerebral distribution of glutamate, glutamine, AMP (Adenosine monophosphate), and GMP (Guanosine monophosphate) levels in the cortex, hippocampus and striatum for CFS mice. Conversely, the levels of GABA (γ-aminobutyric acid) were notably decreased in the hypothalamus, while adenosine levels showed a widespread reduction across various brain microregions with a pronounced decrease observed in the hippocampus. Moreover, choline levels exhibited significant reductions in the striatum, midbrain, and medulla oblongata distributions, and the reduction in choline phosphate levels was mainly concentrated in the vicinity of the striatum (Fig. 10). Alterations in the levels

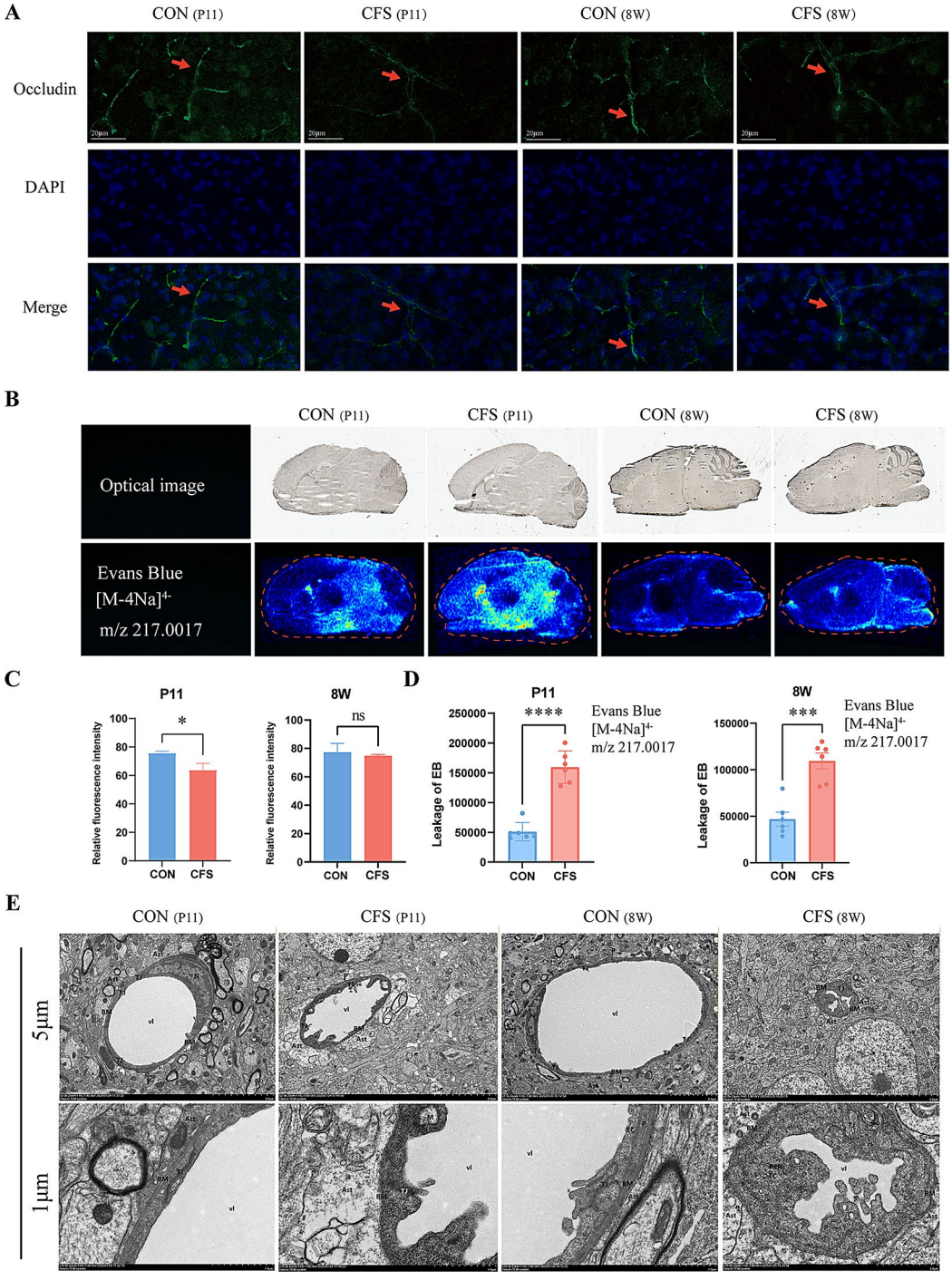

Fig. 9 CFS increased BBB damage in brain tissue of C57 mice. **A**) Immunofluorescence staining of Occludin, the red arrows point to brain microvessels. **B**) Representative images of extravasation of Evans blue. **C**) The expression of occludin was quantitatively analyzed in different groups stained in immunofluorescence ($n=3$). **D**)The content of tracer EB in each group was quantitatively analyzed ($n=6$). **E**) Representative transmission electron microscope images of BBB structure ($n=3$)

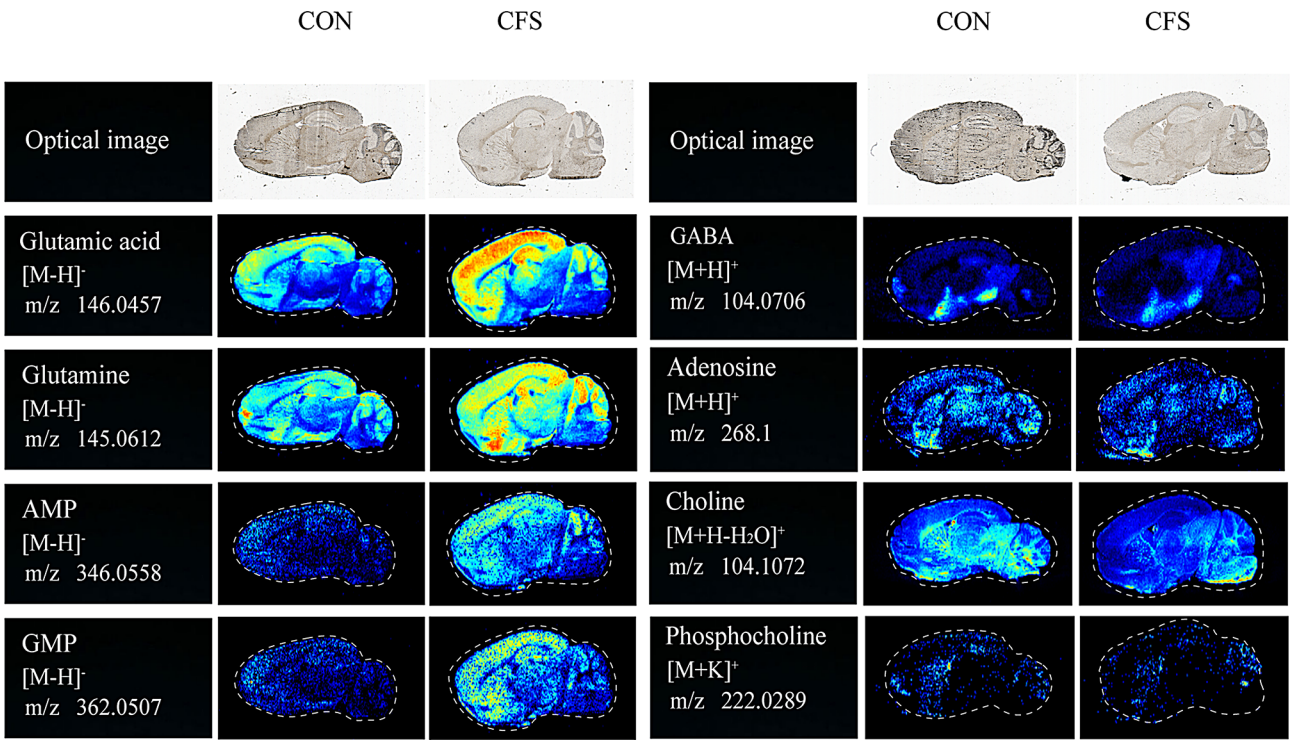

Fig. 10 Spatial distribution of neurotransmitters and other metabolites in the brain of CFS mice

of these metabolites can influence neuronal excitability, potentially triggering epileptic seizures [27, 28]. It is well known that BBB destruction causes an imbalance in ionic homeostasis, which can lead to abnormal neuronal firing and thus affect neurotransmitter synthesis or release [29]. Consequently, this evidence confirms that experiencing CFS in infancy can lead to changes in the distribution of specific neurotransmitters and metabolites in the brain.

Dysregulating the ECM-receptor interaction increases epilepsy susceptibility in mice

To further verify the reliability of regulating the ECM-receptor interaction signaling pathway in increasing susceptibility to epilepsy in mice, we conducted additional validation experiments, the steps of which are shown in (Fig. 11A). Normal C57 wild-type mice (8w) were selected and divided into NaCl and Incyclinide groups. Their lateral ventricles were injected with NaCl or Incyclinide respectively, followed by subthreshold stimulation with PTZ (40 mg/kg), and the convulsive behavior of the mice was observed within 30 min. Incyclinide is a matrix metalloproteinases (MMP) inhibitor that can induce dynamic remodeling of ECM and inhibit angiogenesis. Subsequently, to validate the accuracy of our lateral ventricle localization, we conducted microinjections into the lateral ventricle using the vital tracer EB (Fig. 11B). Continuous EEG recording and simultaneous video monitoring revealed that all the mice in the group injected with Incyclinide developed grand mal seizures, both with shorter latency and longer duration, compared with the NaCl group ($n = 8$, Fig. 11G ~ I). As well as the grades and power of ictal EEG activity during seizures were also higher than that of the NaCl group (Fig. 11C ~ F). If we marked the start time after the lateral ventricle microinjection intervention, compared with NaCl group, the latency period of grade V grand mal seizure was shortened from 1578 ± 543.79 s to -143.7 ± 421.01 s, and the duration of grand mal seizure was increased from 3.67 ± 8.98 s to 20.67 ± 7.37 s (Fig. 11H ~ I). These findings indicate that the Incyclinide disrupts the ECM-receptor interaction signaling pathway, resulting in a substantial reduction in the threshold for convulsive seizures and heightened susceptibility to epilepsy in mice.

Discussion

Dysfunction of the BBB can result in neuronal damage, potentially leading to epileptic changes [29, 30]. Current research on susceptibility to post-convulsive epilepsy has primarily focused on epigenetic mechanisms, proteases, and inflammation-related genes [30, 31], while the specific effects of the BBB on adult epilepsy susceptibility and the underlying molecular mechanisms remains unknown. Our study is the first to investigate this relationship, revealing from the perspective of blood-brain barrier proteomics that dysregulation of the ECM-receptor interaction signaling pathway is the key to increased susceptibility to epilepsy after CFS.

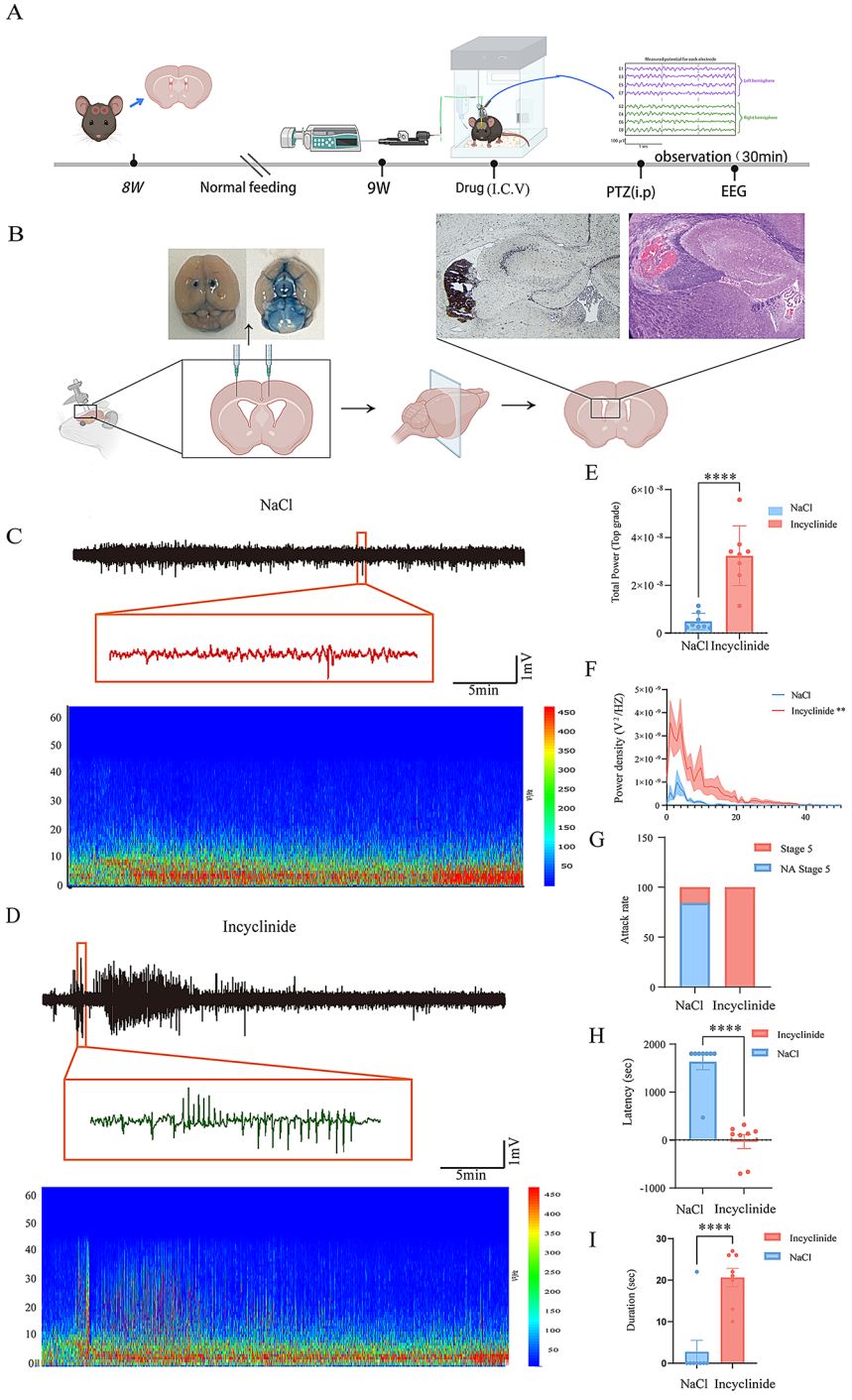

Fig. 11 Incyclinide increase susceptibility to epilepsy. (**A**) Flow chart of drug administration in the lateral ventricle of the inhibitor. (**B**) Evans Blue verified lateral ventricle localization. (**C-D**) Heat maps of maximum EEG power spectra within 30 min after PTZ intervention in the NaCl group and the Incyclinide group. (**E-F**) Maximum EEG total power and power density within 30 min after PTZ intervention in NaCl group and incyclinide group ($n=8$). (**G-I**) After microinjection of incyclinide and 40 mg/kg PTZ, the proportion, latency and duration of grade V recurrent seizures were evaluated according to Racine classification ($n=8$)

To investigate adult seizure susceptibility, PTZ (40 mg/kg) as a subthreshold stimulus [32] was administered to 8 weeks old mice. The study found that 66.7% of CFS mice developed grade V seizures in adulthood, compared to none of mice in control group (Fig. 1D). Only 37.5% of mice in the control group developed grade III seizures (Fig. 1D). Additionally, the model group had significantly shorter latency and longer duration of grade V seizures

($P < 0.01$, Fig. 1E ~ F). These findings, consistent with Kawano et al. [15], suggest childhood CFS may increase epileptic susceptibility in adulthood.

We successfully prepared brain capillaries, which are suitable for BBB proteomic studies (Figs. 2 and 3A). Based on the BBB proteomic data and the bioinformatic analysis indicated that ECM-receptor interaction and integrin-mediated signaling pathway ($P < 0.01$) were enriched significantly in CFS mice (Fig. 4 ~ 5). The ECM signaling pathway is integral to tissue and organ morphogenesis [33, 34]. Alterations in this pathway's components not only affect the BBB remodeling but also influence the cellular functions. The integrin gene family, acting as ECM receptors, is pivotal in regulating intracellular signaling to coordinate cellular responses to environmental changes through outside-in signaling [35]. Therefore, these findings have significant implications that ECM-receptor interaction pathway could underlie the epileptic susceptibility of CFS.

Based on the proteomic data, we found the first nine hub genes in the PPI network of 53 DEPs included members of the collagen family (Col4a5, Col4a6) in the ECM-receptor interaction pathway, as well as three members of the integrin family (Itgb4, Itga6, and Itga8). It is worth mentioning that the important tight junction proteins Cldn5 and Ocln, as well as aquaporin Aqp4, were present in the network (Fig. 6). Itga8 is responsible for controlling the recruitment of mesenchymal cells into epithelial structures, facilitating intercellular interactions, and regulating the growth of synapses in sensory and motor neurons. Research has confirmed that endothelial cells and astrocytes play a crucial role in secreting ECM proteins to create and uphold basement membranes [36, 37]. Cldn5 is responsible for regulating the size-selectivity of the BBB by forming connections between cerebral vascular endothelial cells. Disruption of Cldn5 leads to compromised BBB integrity [38, 39]. In contrast, Occludin plays a direct role in the barrier function of the BBB by binding to neighboring cells and facilitating paracellular closure, affecting transmembrane resistance [40]. Aqp4, predominantly expressed in astrocyte peduncles, is crucial for controlling the exchange of water molecules across the BBB and brain-cerebrospinal fluid interface [41]. The close interaction between the ECM and the BBB cells creates an ideal system for maintaining barrier integrity [42]. It can be concluded that damage to the cellular matrix and TJ-related proteins can impair the BBB to some extents, leading to an imbalance of homeostasis in the brain. It was reported that intact ECM can inhibit the onset of seizures [43]. Hence, it is clear that these genes are associated with an increased risk of developing epilepsy in adulthood through their impact on BBB.

The expression levels of protein and mRNA of all the aforementioned proteins were down-regulated (Fig. 7). Disruptions in the expression of ECM proteins have been linked to potential changes in endothelial cell behavior, resulting in persistent damage and dysfunction of the microvascular system, ultimately affecting the integrity of the BBB [36]. As a result, we have put forward a novel hypothesis suggesting that epilepsy susceptibility in adults may be influenced, at least in part, by the down-regulation of the proteins in ECM-receptor interaction pathway.

To validate our hypothesis, we selected Incyclinide to dysregulate the ECM-receptor interaction signaling pathway. Lateral ventricular injection of drugs allows direct access to the cerebrospinal fluid and easier penetration of the drug into the brain parenchyma through exchange interactions between the cerebrospinal fluid and brain tissue [44, 45]. Compared with the NaCl group, the epilepsy susceptibility threshold of the Incyclinide treatment group was significantly reduced, and the severity of seizures was significantly increased (Fig. 11C-I). Under physiological conditions, MMPs are crucial for maintaining BBB integrity and CNS homeostasis through dynamic regulation of ECM remodeling [46, 47]. Several studies demonstrate that MMP-mediated proteolysis drives the structural and functional changes that occur during the development and homeostasis of the CNS [48–51]. Incyclinide, by inhibiting MMP activity, disrupts ECM remodeling, leading to homeostatic imbalance in the brain and interfering with cell migration, proliferation, and repair processes within the CNS. Hence, the study provided additional insights, highlighting the pivotal role of ECM-receptor interaction signaling pathway dysregulation in epilepsy susceptibility.

While our experiments show evidence of partial BBB recovery in adult CFS mice compared to infancy, the BBB remains significantly dysfunctional (Fig. 9). Metabolic homeostasis is imbalanced after BBB disruption, resulting in alterations to the distribution of metabolites within the brain. In our MSI study, we observed elevated levels of glutamate, glutamine, AMP, and GMP in the cortex, hippocampus, and striatum of CFS mice. Conversely, we found decreased levels of GABA in the hypothalamus and adenosine in the hippocampus in these mice (Fig. 10). It has been reported that when the BBB is disrupted, glutamate (a major excitatory neurotransmitter) transporter proteins and catalytic enzymes are altered, and the excessive release of glutamate leads to neuronal hyperexcitability, which in turn leads to epilepsy [52, 53]. BBB strictly regulates the entry and exit of substances, particularly amino acid neurotransmitters, of which GABA is the principal inhibitory neurotransmitter in the CNS, and a decrease in GABA-mediated inhibitory synaptic transmission has been clinically associated with epilepsy [54]. Adenosine also plays a role in regulating the activity of immune cells that are crucial for the

remodeling and upkeep of the ECM [55]. It's worth noting that ECM not only offers structural support to the cell, but also communicates signals through its receptors, such as integrins, to regulate cellular activities, such as neurotransmitter synthesis and release [56]. In pathological states, abnormal remodeling of the ECM may lead to the accumulation of neurotransmitter metabolites such as phosphocholine, and imbalances in these metabolites have been associated with the development of neurological disorders [57]. The above studies suggest to us that BBB disruption alters brain metabolites associated with neuronal excitability.

Limitations: The current study investigated BBB proteomic alterations associated with epilepsy susceptibility exclusively resulting from FS in the absence of other contributing factors. The mechanisms underlying epilepsy susceptibility in cases of FS combined with genetic predisposition or infectious etiologies are likely to be more complex and are not addressed in this work. While we identified dysregulation of the ECM-receptor interaction pathway as a key factor in increased epilepsy susceptibility, further research is needed to investigate the exact mechanisms by which the ECM affects susceptibility. Besides, other potentially relevant pathways, including focal adhesion and mRNA export from nucleus, were identified but not investigated in depth (Fig. 5A and Fig. S3).

Conclusion

Our findings indicate that mice experienced CFS in infancy increased susceptibility to epilepsy in adulthood. BBB proteomic profile was significantly altered in the CFS mice, and revealed that dysregulation of the ECM-receptor interaction pathway was a key mechanism for the increased susceptibility to epilepsy. The expression levels of protein and mRNA of the proteins related to ECM-receptor interaction pathway were down-regulated, meanwhile, the distribution of neuroexcitatory metabolites within the brain was altered. Subsequent validation experiments showed that dysregulation of the ECM-receptor interaction signaling pathway exacerbated epilepsy susceptibility in adult mice. These findings may help to elucidate the role of BBB alterations in the progression of epilepsy susceptibility, and provide new targets for subsequent prevention and treatment of epilepsy.

Abbreviations

BBB	Blood-brain barrier
CNS	Central nervous system
CFS	Complex febrile seizures
PTZ	Pentylenetetrazole
DEPS	Differentially expressed proteins
MSI	Mass spectrometry imaging
AMP	Adenosine monophosphate
GMP	Guanosine monophosphate
FS	Febrile seizures
TJs	Tight junctions
ECM	Extracellular matrix
MMP	Matrix Metalloproteinases
EB	Evans Blue

Supplementary Information

The online version contains supplementary material available at https://doi.org/10.1186/s12987-025-00660-x.

Supplementary Material 1: Fig S1. Changes in body weight from infancy to adult in each group of mice. Fig S2. Changes in expression of proteins enriched for ECM-receptor interaction and integrin-mediated signaling pathway. A) Expression changes of proteins enriched for integrin-mediated signaling pathway. B) Expression changes of proteins enriched for ECM-receptor interaction. Fig S3. GO analysis of all DEPs in CFS mice.

Supplementary Material 2

Supplementary Material 3

Author contributions

Dezhi Kong, Jianghua Zhang and Wei Zhang: designing the research and experiments; Qian Wang: conducting experiments, image processing and preparing the manuscript; Qian Wang, Liangyu Pan, Siruan Chen and Yuyu Zhang: analyzing the data; Qian Wang, Guangyuan Liu and Yiying Wu: MSI data acquisition; Xia Qian and Panpan Zhang: image processing; Dezhi Kong and Jianghua Zhang: revising the manuscript. All authors reviewed the manuscript.

Funding

This study received partial financial support in the form of the National Natural Science Foundation of China (No. 82174004 and 82474103) and the National Key Research and Development Program of China for Modernization of Traditional Chinese Medicine (No. 2022YFC3500500).

Data availability

Data is provided within the manuscript or supplementary information files.

Declarations

Ethics approval and consent to participate

Animal studies complied with the Animal Care guidelines, which were approved by the Institutional Animal Care and Use Committee at Hebei Medical University (Approval Number: IACUC-Hebmu-2021022, Shijiazhuang, China). These experiments were performed in accordance with the National Institutes of Health Guidelines for the Care and Use of Laboratory Animals.

Consent for publication

All authors gave their consent for publication.

Competing interests

The authors declare no competing interests.

Author details

[1]Institute of Integrative Medicine, College of Chinese Integrative Medicine, Hebei Medical University, Shijiazhuang, China
[2]Key Laboratory of Tranquilizing TCM, Hebei Provincial Administration of Traditional Chinese Medicine, Shijiazhuang 050017, China
[3]Key Laboratory of Neural and Vascular Biology, Ministry of Education of China, Shijiazhuang, China

Received: 30 September 2024 / Accepted: 2 May 2025
Published online: 13 May 2025

References

1. Han JY, Han SB. Pathogenetic and etiologic considerations of febrile seizures. Clin Exp Pediatr. 2023;66(2):46–53.
2. Baram TZ, Gerth A, Schultz L. Febrile seizures: an appropriate-aged model suitable for long-term studies. Brain Res Dev Brain Res. 1997;98(2):265–70.

3. Chiang LM, Huang GS, Sun CC, Hsiao YL, Hui CK, Hu MH. Association of developing childhood epilepsy subsequent to febrile seizure: A population-based cohort study. Brain Dev. 2018;40(9):775–80.
4. Jongruk P, Wiwattanadittakul N, Katanyuwong K, Sanguansermsri C. Risk factors of epilepsy in children with complex febrile seizures: A retrospective cohort study. Pediatr Int. 2022;64(1):e14926.
5. Biltz S, Speltz L. Febrile seizures. Pediatr Ann. 2023;52(10):e388–93.
6. Ben-Zvi A, Liebner S. Developmental regulation of barrier- and non-barrier blood vessels in the CNS. J Intern Med. 2022;292(1):31–46.
7. Marc T. Brain development and the immune system: an introduction to inflammatory and infectious diseases of the child's brain. Handb Clin Neurol. 2013;112:1087–9.
8. Hashimoto Y, Greene C, Munnich A, Campbell M. The CLDN5 gene at the blood-brain barrier in health and disease. Fluids Barriers CNS. 2023;20(1):22.
9. Mosili P, Maikoo S, Mabandla MV, Qulu L. The pathogenesis of Fever-Induced febrile seizures and its current state. Neurosci Insights. 2020;15:1489267155.
10. Scott RC. What are the effects of prolonged seizures in the brain? Epileptic Disord. 2014;16(1):S6–11.
11. Ransohoff RM. Immunology: barrier to electrical storms. Nature. 2009;457(7226):155–6.
12. Reiss Y, Bauer S, David B, Devraj K, Fidan E, Hattingen E, Liebner S, Melzer N, Meuth SG, Rosenow F, Ruber T, Willems LM, Plate KH. The neurovasculature as a target in Temporal lobe epilepsy. Brain Pathol. 2023;33(2):e13147.
13. Ogata S, Ito S, Masuda T, Ohtsuki S. Changes of Blood-Brain barrier and brain parenchymal protein expression levels of mice under different Insulin-Resistance conditions induced by High-Fat diet. Pharm Res. 2019;36(10):141.
14. Pardridge WM. Blood-brain barrier genomics. Stroke. 2007;38(2 Suppl):686–90.
15. Kawano S, Itoh K, Ishihara Y. Suppressive effects of docosahexaenoic acid intake on increased seizure susceptibility after growth due to febrile seizures in infancy. Biol Pharm Bull. 2023;46(9):1184–93.
16. Feng B, Tang Y, Chen B, Xu C, Wang Y, Dai Y, Wu D, Zhu J, Wang S, Zhou Y, Shi L, Hu W, Zhang X, Chen Z. Transient increase of interleukin-1beta after prolonged febrile seizures promotes adult epileptogenesis through long-lasting upregulating endocannabinoid signaling. Sci Rep. 2016;6:21931.
17. van Gassen KL, Hessel EV, Ramakers GM, Notenboom RG, Wolterink-Donselaar IG, Brakkee JH, Godschalk TC, Qiao X, Spruijt BM, van Nieuwenhuizen O, de Graan PN. Characterization of febrile seizures and febrile seizure susceptibility in mouse inbred strains. Genes Brain Behav. 2008;7(5):578–86.
18. Griflyuk AV, Postnikova TY, Zaitsev AV. Animal models of febrile seizures: limitations and recent advances in the field. Cells. 2024;13(22):1895.
19. Ogata S, Ito S, Masuda T, Ohtsuki S. Efficient isolation of brain capillary from a single frozen mouse brain for protein expression analysis. J Cereb Blood Flow Metab. 2021;41(5):1026–38.
20. Lee YK, Uchida H, Smith H, Ito A, Sanchez T. The isolation and molecular characterization of cerebral microvessels. Nat Protoc. 2019;14(11):3059–81.
21. Yu R, Liu H, Wang B, Harvey PJ, Wei N, Chu Y. Synthesis and biological activity study of the retro-isomer of RhTx against TRPV1. RSC Adv. 2020;10(4):2141–5.
22. He J, Huang L, Tian R, Li T, Sun C, Song X, Lv Y, Luo Z, Li X, Abliz Z. MassImager: A software for interactive and in-depth analysis of mass spectrometry imaging data. Anal Chim Acta. 2018;1015:50–57.
23. Zhang Y, Chen K, Sloan SA, Bennett ML, Scholze AR, O'Keeffe S, Phatnani HP, Guarnieri P, Caneda C, Ruderisch N, Deng S, Liddelow SA, Zhang C, Daneman R, Maniatis T, Barres BA, Wu JQ. An RNA-sequencing transcriptome and splicing database of glia, neurons, and vascular cells of the cerebral cortex. J Neurosci. 2014;34(36):11929–47.
24. Chen C, Chen J, Wang Y, Fang L, Guo C, Sang T, Peng H, Zhao Q, Chen S, Lin X, Wang X. Ganoderma lucidum polysaccharide inhibits HSC activation and liver fibrosis via targeting inflammation, apoptosis, cell cycle, and ECM-receptor interaction mediated by TGF-beta/Smad signaling. Phytomedicine. 2023;110:154626.
25. Wang R, Zhu Y, Liu Z, Chang L, Bai X, Kang L, Cao Y, Yang X, Yu H, Shi MJ, Hu Y, Fan W, Zhao BQ. Neutrophil extracellular traps promote tPA-induced brain hemorrhage via cGAS in mice with stroke. Blood. 2021;138(1):91–103.
26. Gruenbaum BF, Zlotnik A, Fleidervish I, Frenkel A, Boyko M. Glutamate neurotoxicity and destruction of the Blood-Brain barrier: key pathways for the development of neuropsychiatric consequences of TBI and their potential treatment strategies. Int J Mol Sci. 2022;23(17):9628.
27. Jin B, Pang X, Zang Q, Ga M, Xu J, Luo Z, Zhang R, Shi J, He J, Abliz Z. Spatiotemporally resolved metabolomics and isotope tracing reveal CNS drug targets. Acta Pharm Sin B. 2023;13(4):1699–710.
28. Pang X, Gao S, Ga M, Zhang J, Luo Z, Chen Y, Zhang R, He J, Abliz Z. Mapping metabolic networks in the brain by ambient mass spectrometry imaging and metabolomics. Anal Chem. 2021;93(17):6746–54.
29. Janigro D. Are you in or out? Leukocyte, ion, and neurotransmitter permeability across the epileptic blood-brain barrier. Epilepsia. 2012;53(Suppl 1):26–34.
30. Wu D, Feng B, Dai Y, Wu X, Chen B, Xu C, Tang Y, Wang K, Zhang S, Shuangwang, Luo B, Chen Z. Corrigendum to Intergenerational Transmission of Enhanced Seizure Susceptibility after Febrile Seizures. EBioMedicine. 2017;17:206–215.
31. Song W, Bian WJ, Li H, Guo QH, Wang J, Tang B, Zhang JY, Wei W, Liu XR, Liao WP, Li B, He N. IFIH1 variants are associated with generalised epilepsy preceded by febrile seizures. J Med Genet. 2024;61(9):895–903.
32. Hill-Yardin EL, Argyropoulos A, Hosie S, Rind G, Anderson P, Hannan AJ, O'Brien TJ. Reduced susceptibility to induced seizures in the Neuroligin-3(R451C) mouse model of autism. Neurosci Lett. 2015;589:57–61.
33. Rosso F, Giordano A, Barbarisi M, Barbarisi A. From cell-ECM interactions to tissue engineering. J Cell Physiol. 2004;199(2):174–80.
34. Daley WP, Peters SB, Larsen M. Extracellular matrix dynamics in development and regenerative medicine. J Cell Sci. 2008;121(Pt 3):255–64.
35. Kamranvar SA, Rani B, Johansson S. Cell cycle regulation by Integrin-Mediated adhesion. Cells. 2022;11(16):2521.
36. Baeten KM, Akassoglou K. Extracellular matrix and matrix receptors in blood-brain barrier formation and stroke. Dev Neurobiol. 2011;71(11):1018–39.
37. Hynes RO, Naba A. Overview of the matrisome–an inventory of extracellular matrix constituents and functions. Cold Spring Harb Perspect Biol. 2012;4(1):a4903.
38. Ronaldson PT, Davis TP. Regulation of blood-brain barrier integrity by microglia in health and disease: A therapeutic opportunity. J Cereb Blood Flow Metab. 2020;40(1suppl):S6–24.
39. Greene C, Hanley N, Reschke CR, Reddy A, Mäe MA, Connolly R, Behan C, O Keeffe E, Bolger I, Hudson N, Delaney C, Farrell MA, Brien O, Cryan DF, Brett J, Beausang FM, Betsholtz A, Henshall C, Doherty DC, Campbell CP. M. Microvascular stabilization via blood-brain barrier regulation prevents seizure activity. Nat Commun. 2022;13(1):2003.
40. Zhang R, Liu Y, Chen D, Tang Y. The role of occludin in vascular barrier function in vivo: do we need to re-examine? Crit Care. 2020;24(1):455.
41. Jeon H, Kim M, Park W, Lim JS, Lee E, Cha H, Ahn JS, Kim JH, Hong SH, Park JE, Lee EJ, Woo CW, Lee S. Upregulation of AQP4 improves Blood-Brain barrier integrity and perihematomal edema following intracerebral hemorrhage. Neurotherapeutics. 2021;18(4):2692–706.
42. Wang ZB, Qu J, Xie P, Yang ZQ, Mao CX, Zhang Y, He ZW, Yang ZY, Mao XY, Liu ZQ. Integrative analysis of expression profile indicates the ECM receptor and LTP dysfunction in the glioma-related epilepsy. BMC Genomics. 2022;23(1):430.
43. Patel DC, Tewari BP, Chaunsali L, Sontheimer H. Neuron-glia interactions in the pathophysiology of epilepsy. Nat Rev Neurosci. 2019;20(5):282–97.
44. Saleh SR, Khamiss SE, Aly MS, Khattab SN, Sheta E, Elnozahy FY, Thabet EH, Ghareeb DA, Awad D, El-Bessoumy AA. Biochemical investigation and in Silico analysis of the therapeutic efficacy of Ipriflavone through Tet-1 Surface-Modified-PLGA nanoparticles in Streptozotocin-Induced Alzheimer's like disease: reduced oxidative damage and etiological descriptors. Int J Pharm. 2025;669:125021.
45. Li X, Zhang Y, Chang J, Zhang C, Li L, Dai Y, Yang H, Wang Y. Mfsd2a attenuated hypoxic-ischemic brain damage via protection of the blood-brain barrier in mfat-1 Transgenic mice. Cell Mol Life Sci. 2023;80(3):71.
46. Overall CM. Molecular determinants of metalloproteinase substrate specificity: matrix metalloproteinase substrate binding domains, modules, and exosites. Mol Biotechnol. 2002;22(1):51–86.
47. Rodriguez D, Morrison CJ, Overall CM. Matrix metalloproteinases: what do they not do? New substrates and biological roles identified by murine models and proteomics. Biochim Biophys Acta. 2010;1803(1):39–54.
48. Nagy V, Bozdagi O, Matynia A, Balcerzyk M, Okulski P, Dzwonek J, Costa RM, Silva AJ, Kaczmarek L, Huntley GW. Matrix metalloproteinase-9 is required for hippocampal late-phase long-term potentiation and memory. J Neurosci. 2006;26(7):1923–34.
49. Gorkiewicz T, Balcerzyk M, Kaczmarek L, Knapska E. Matrix metalloproteinase 9 (MMP-9) is indispensable for long term potentiation in the central and basal but not in the lateral nucleus of the amygdala. Front Cell Neurosci. 2015;9:73.
50. Bozdagi O, Nagy V, Kwei KT, Huntley GW. In vivo roles for matrix metalloproteinase-9 in mature hippocampal synaptic physiology and plasticity. J Neurophysiol. 2007;98(1):334–44.

51. Bijata M, Labus J, Guseva D, Stawarski M, Butzlaff M, Dzwonek J, Schneeberg J, Bohm K, Michaluk P, Rusakov DA, Dityatev A, Wilczynski G, Wlodarczyk J, Ponimaskin E. Synaptic remodeling depends on signaling between serotonin receptors and the extracellular matrix. Cell Rep. 2017;19(9):1767–82.
52. Smith QR. Transport of glutamate and other amino acids at the blood-brain barrier. J Nutr. 2000;130(4S Suppl):S1016–22.
53. Aaslid R. Cerebral autoregulation and vasomotor reactivity. Front Neurol Neurosci. 2006;21:216–228.
54. Akyuz E, Polat AK, Eroglu E, Kullu I, Angelopoulou E, Paudel YN. Revisiting the role of neurotransmitters in epilepsy: an updated review. Life Sci. 2021;265:118826.
55. Beamer E, Kuchukulla M, Boison D, Engel T. ATP and adenosine-Two players in the control of seizures and epilepsy development. Prog Neurobiol. 2021;204:102105.
56. Dahal SS, Bastola S, Dayal S, Yau S, Ramamurthi J. Stem cell based approaches to modulate the matrix milieu in vascular disorders. Front Cardiovasc Med. 2022;9:879977.
57. Cunnane SC, Trushina E, Morland C, Prigione A, Casadesus G, Andrews ZB, Beal MF, Bergersen LH, Brinton RD, de la Monte S, Eckert A, Harvey J, Jeggo R, Jhamandas JH, Kann O, la Cour CM, Martin WF, Mithieux G, Moreira PI, Murphy MP, Nave KA, Nuriel T, Oliet S, Saudou F, Mattson MP, Swerdlow RH, Millan MJ. Brain energy rescue: an emerging therapeutic concept for neurodegenerative disorders of ageing. Nat Rev Drug Discov. 2020;19(9):609–33.

Publisher's note